UNIVERSITY OF CALIFORNIA

Santa Barbara

The Hillslope Signature of Knickpoints Resulting from Stream Capture, Coastal Processes, and Resistant Bedrock on Santa Cruz Island, CA: Insights from an Automated Knickpoint-Selection Algorithm

A Thesis submitted in partial satisfaction of the

requirements for the degree Master of Science in Geological Sciences

by

Alexander Banks Neely

Committee in charge:

Professor Douglas Burbank, Chair

Professor Alexander Simms

Professor Edward Keller

September 2015

The thesis of Alexander Banks Neely is approved.

_____

Edward Keller

_____

Alexander Simms

_____

Douglas Burbank, Committee Chair

June 2015

ACKNOWLEDGEMENTS

I would like to extend thanks to my advising committee: Doug Burbank for helpful reviews and Bodo Bookhagen for project development and vision. I would like to thank the US Geological Survey for the collection of the airborne lidar dataset, also John Potapenko for his work preparing the lidar DEM. I will make a quick shout out to John Cougar Mellancamp, Jay-Z, the soundtrack to all of the Rocky movies, and Jeremy Sasshole for their musical inspiration throughout this research project. In addition, I would like to thank Ed Keller, Alex Simms, Eric Schoettle, Aaron Bufe, John Harvey, Paul Alessio, and Shelby Fredrickson for useful discussion.

ABSTRACT

Insights from an Automated Knickpoint Selection Algorithm: The Hillslope Signature of Knickpoints Resulting from Stream Capture, Coastal Processes, and Resistant Bedrock on Santa Cruz Island, CA

by

Alexander Banks Neely

Oversteepened, convex segments of stream channels called knickpoints have been utilized as markers that commonly migrate upstream and delineate abrupt changes in erosional efficiency influenced by base-level fall, changes in rock strength, or strong spatial variations in discharge. Currently, few analyses based on DEMs enable discrimination among migrating knickpoints related to changes in external forcing (baselevel fall, stream capture, and climate) versus fixed knickpoints related to internal forcing within a catchment (resistant bedrock units, coarse debris flow run-outs at tributary junctions, or landslide dams). Furthermore, few analyses have characterized the extent that migratory knickpoints steepen downstream-adjacent hillslopes. To study these interactions, we exploit a 1-m resolution LiDAR DEM of Santa Cruz Island (SCI), CA and a new algorithm that automatically extracts and measures the dimensions of any knickpoint in a regional DEM. The algorithm reduces knickpoint selection time by >99% and removes selection bias from the traditional means of regional knickpoint identification that relies on visual inspections of individual longitudinal profiles.

The spatial pattern of knickpoints located by the algorithm highlight three dominant knickpoint-forming processes on SCI: knickpoints fixed to contacts between rocks of different strength, knickpoints migrating upstream from an incision pulse caused by a significant stream capture event, and mobile knickpoints stemming from relative sea-level fall and wave erosion of sea-cliffs. Nearly 36% of the hillslope area downstream from migratory knickpoints has slopes above threshold values of 35˚, and on average, these regions display a 4-6˚ steeper median hillslope-gradient than hillslopes upstream from migratory knickpoints. Hillslope-gradient histograms are nearly identical upstream and downstream from knickpoints fixed to spatial changes in rock strength or when re-analyzing hillslopes surrounding migratory knickpoints with a 10-m resolution DEM. From regionally extensive map of stream knickpoints, geological context, and hillslope attributes extracted from a 1-m resolution DEM, new insights emerge on the controls of landscape evolution; insights that would be much harder to obtain through individual knickpoint selection or lower resolution imagery.

Introduction

A. *Background*

Empirical evidence suggests that streams equilibrated to a static baselevel, discharge pattern, and bedrock strength commonly exhibit a form described by a power-law relationship between local channel slope and contributing drainage area: $S = k_s A^{\theta}$ [*Hack,* 1957*; Flint,* 1974], where S = local channel slope, A = contributing drainage area, and k_s (stream steepness) and θ (stream concavity) are constants, with θ typically ranging between 0.4 and 0.6 [*Kirby and Whipple,* 2012]. Knickpoints and knickzones represent a deviation from the slope- and drainage area- dependent stream-power model (Fig. 1). In such localities, stream gradient is significantly greater than expected for the respective contributing drainage area, thereby creating a convexity in an otherwise concave-up longitudinal stream profile. These convexities could be locally steepened zones such as waterfalls [*Baldwin,* 2003*; Bishop et al.,* 2005*; Crosby and Whipple,* 2006*; Mackey et al.,* 2014*; Dibiase et al,* 2014] or could define a sustained change in the power-law relation between channel slope and drainage area (increase in k_s, stream steepness) [*Wobus et al,* 2006a*; Harkins et al.,* 2007*; Berlin and Anderson,* 2007*; Miller et al,* 2012*; Miller et al,* 2013]. Locally steepened zones, upstream and downstream of which k_s does not vary, are called 'vertical step knickpoints', whereas sustained steepened zones where k_s increases from upstream to downstream reaches are called 'slope-break knickpoints' [*Kirby and Whipple,* 2012]. If multiple knickpoints are spaced closely together, a 'knickzone' can form where k_s progressively increases towards the mouth of a steam or the confluence of a tributary with a main channel (Fig. 1) [*Lague,* 2014]. Commonly, acceleration of streamflow over top of a knickpoint lip increases shear stress upstream of the knickpoint, thus creating a steepened reach called a 'drawdown reach' which extends upstream from a

knickpoint lip [*Gardner,* 1983*; Berlin and Anderson,* 2009*; Lamb et al.,* 2015]. If knickpoint retreat is sufficiently rapid and/or if the knickpoint lip is undercut by the base of a waterfall and destabilized before establishment of a drawdown reach, the knickpoint will persist as a discrete point (Fig. 1 insets).

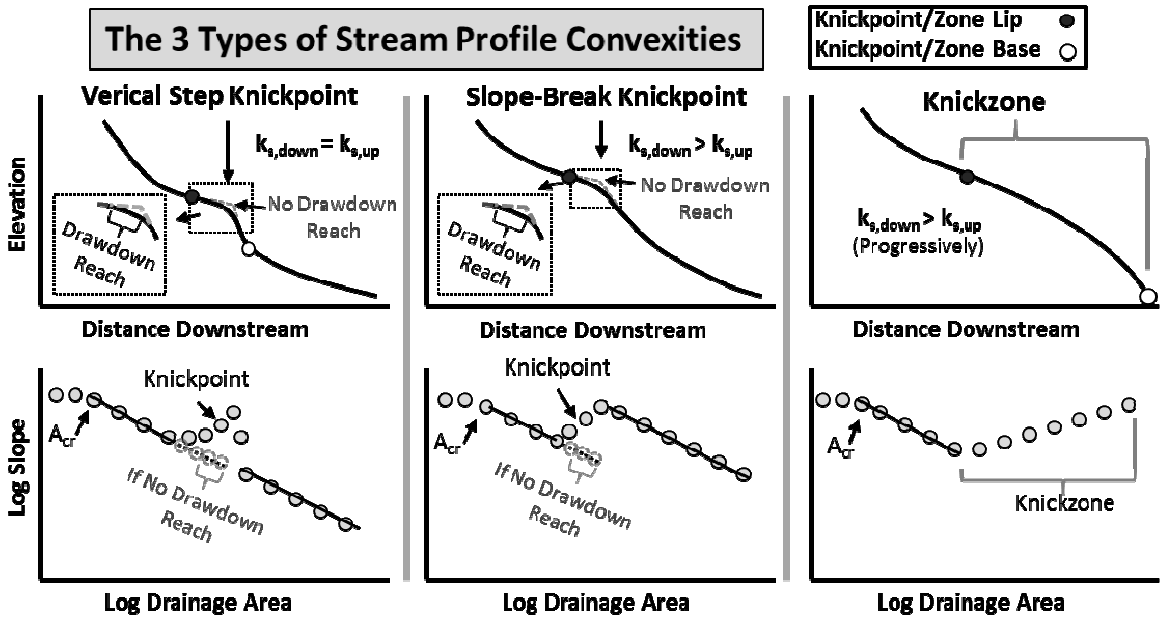

Figure 1) Three different convexity forms for knickpoints: vertical step (A); slope-break (B) and knickzones (C) in elevation/distance space (top) and log slope/log area space (bottom). A_{cr} (critical area) highlights a change in the log slope/log area relationship that typically defines a transition from hillslope/colluvial processes to the fluvial network. $k_{s,down}$ refers to the channel steepness downstream of the knickpoint, and $k_{s,up}$ refers to the channel steepness upstream from the knickpoint. Knickpoints may develop a drawdown reach (see insets) extending upstream, or may persist as a discrete point. Geometric differences are shown between discrete knickpoints (grey dashed lines) and knickpoints with drawdown reaches. Note knickpoints typically only span scales of a few hundred meters, whereas knickzones can span a few kilometers to tens of kilometers. [*After Lague,* 2014].

Under the assumption that topographic slope is a proxy for erosion rate, slope-break knickpoints and knickzones are commonly interpreted to delineate boundaries between regions experiencing different erosion rates [*Kirby and Whipple,* 2012]. Typically, an overall contrast between a higher erosion rate downstream versus a lower erosion rate upstream from the knickpoint drives migration of these features upstream [*Whipple and Tucker,* 1999]

Because of the oversteepened nature of vertical step knickpoints, slope-break knickpoints, and knickzones, mechanisms such as toppling, block sliding, and plunge-pool drilling exert a stronger influence on erosion processes in these reaches than in stream reaches with more graded flow regimes [*Frankel et al.,* 2007*; Haviv et al.,* 2010*; Lamb et al.,* 2015]. Additionally, stream-channel properties, such as channel width, sediment cover, grain size, and bed roughness, typically change markedly in knickpoints and knickzones, thereby affecting both transport and abrasion relationships [*Dibiase et al., 2014*]. Because we are interested in locating and describing all steepened reaches where stream characteristics commonly differ from graded flow regimes [*Prancevic and Lamb,* 2015], herein we use the term 'knickpoint' to broadly represent all categories of stream convexities: vertical step knickpoints, slope-break knickpoints, and knickzones.

Stream erosion surrounding knickpoints dictates the landscape response rate to external forcing due to changes in tectonics and climate (Fig. 2) [*Whipple and Tucker,* 1999]. However, similar convexities can be generated within a catchment where streams traverse resistant bedrock lithologies (Fig. 3A) [*Miller,* 1991*; Baldwin,* 2003*; Brocard et al.,* 2006*; Marshall and Roering,* 2014] or where landslide dams [*Korup,* 2006] and debris-flow run-outs plug specific stream reaches [*Hanks and Webb,* 2006*; Ouimet et al.,* 2007] (Fig. 3B). Rather than migrate upstream, these 'internally forced' knickpoints can be fixed near a particular geologic contact or at the location of landslide/debris flow deposition. When using knickpoints as markers to record landscape responses to changes in regional driving forces such as tectonics, climate, or human activity, the most relevant knickpoints are externally forced, mobile, and originate at the locus of an abrupt base-level or discharge change (Fig. 2).

Many studies have linked knickpoints to diverse processes that generate perturbations in a fluvial network. In turn, the spatial distribution of these knickpoints has been used to describe significant changes in environmental variables, such as changes in throw rates on faults (Fig. 1A-B) [*Harkins et al.,* 2007*; Whittaker and Boulton,* 2012*; Whittaker and Walker,* 2014*; Dibiase et al.,* 2014], reorganizations of drainage patterns (Fig. 1D) [*Tinkler et al.,* 1994*; Zaprowski et al.,* 2001*; Prince et al.,* 2011], changes in regional climate (Fig. 2D) [*Crosby and Whipple,* 2006*; Abbuehl et al.,* 2011], shifts in land-use practices (Fig. 2D) [*Booth,* 1990], and coastal interactions due to wave erosion and relative sea-level changes (Fig. 2C) [*Synder et al.,* 2002*; Bishop et al.,* 2005*; Castillo et al.,* 2013*; Mackey et al.,* 2014].

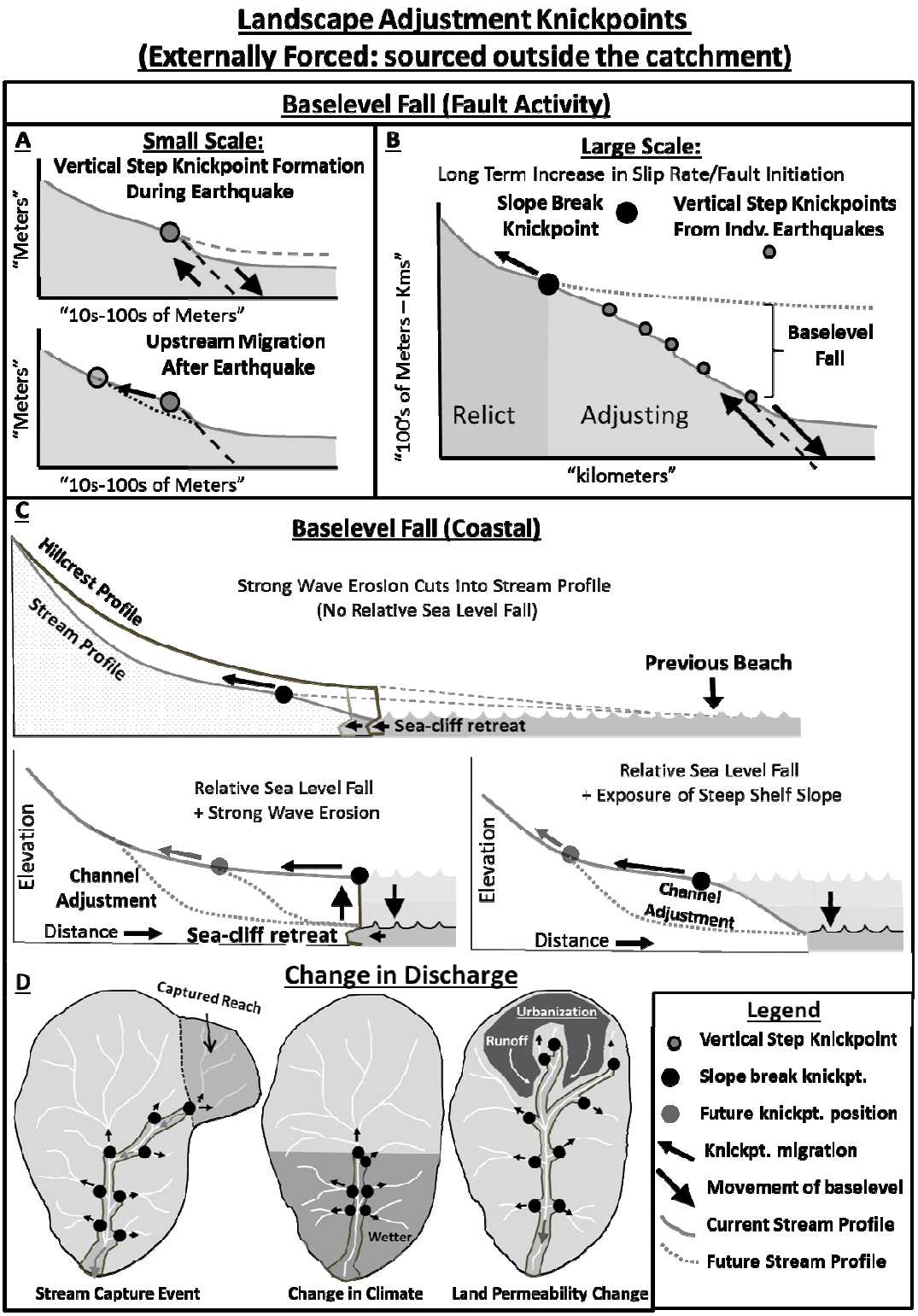

Figure 2) Externally forced (migratory) knickpoints. A) Channel response to base-level fall associated with slip on a fault during an earthquake and subsequent migration of a vertical step knickpoint [*e.g. Yanites and Tucker,* 2010a*; Cook et al.,* 2013]. B) Slope-break knickpoint migrating into relict topography that has not responded to a long-term increase in throw rate on a downstream fault. The reach downstream from the slope-break

knickpoint has many vertical step knickpoints related to repeated earthquakes. C) Coastal knickpoints form from wave erosion shortening a catchment and simulating baselevel fall [*e.g. Mackey et al.,* 2014]. Relative sea-level fall or expose a steep shelf slope also generates a coastal knickpoint. D) Factors that can alter the discharge distribution in a catchment: stream capture, climate change, and urbanization. Stream capture is considered an "external" process because during a discrete capture event, the catchment interacts with additional area that is external from the catchment bounds. Note: more knickpoint generating mechanisms exist but are not shown.

Less research interest has been focused on internally sourced 'fixed' knickpoints [*Miller,* 1991; *Baldwin,* 2003; *Brocard et al.,* 2006; *Hanks and Webb,* 2006; *Ouimet et al.,* 2007, *Marshall and Roering*, 2014; *Wang et al.,* 2014] (Fig. 3). Although highlighting resistant parts of landscapes, because these knickpoints are sourced internally within a catchment, they rarely can be used as direct proxies that relay information upstream pertaining to significant changes in regional tectonics or climate (with the exception of increased landslide activity and a subsequent increase in landslide-dam knickpoint frequency).

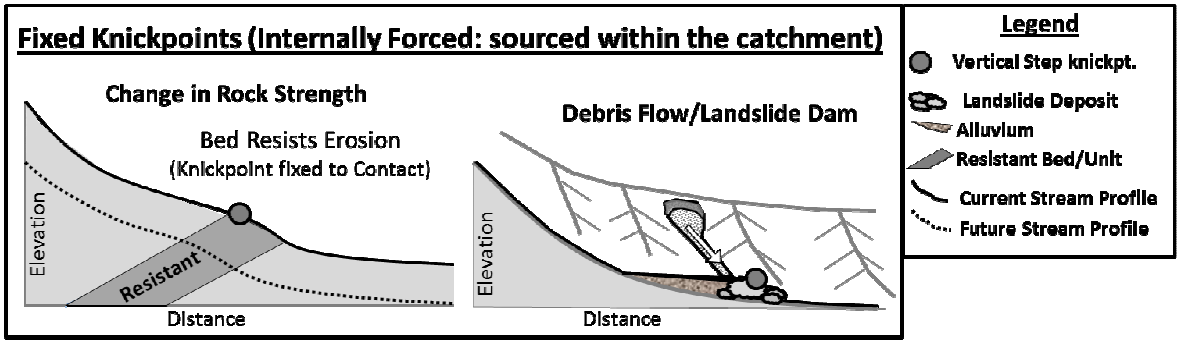

Figure 3) Examples of "Internally forced" knickpoints, or knickpoints developed from erosional process operating within a single catchment. A) Resistant rock unit experiences slower erosion rates than surrounding rock lithologies. B) A landslide-dam plugs stream channel causing upstream aggradation.

Current methods of individual knickpoint extraction limit our ability to efficiently identify and measure knickpoints. These shortcomings restrict the extent and completeness of regional knickpoint maps, and therefore, reduce our ability to identify patterns in knickpoint prevalence, geometry, and surrounding landscape context. Currently, knickpoint definition is commonly performed using a DEM and a digital flow-accumulation array

[*Wobus et al.,* 2006a]. Each channel's longitudinal profile or slope-area plot is analyzed individually, and the analyst manually selects the bounds of the convex segment within each stream that represents a knickpoint. Studies have successfully used this approach to analyze and assess relative rates and patterns of (1) landscape response [*Whittaker et al.,* 2007*; Harkins et al.,* 2007*; Loget et al.,* 2009*; Crosby and Whipple,* 2006*, ect..*], (2) uplift [*Kirby and Whipple,* 2012*; Whittaker et al.,* 2014], and (3) spatial erosion [*Miller et al.,* 2013*; Dibiase et al.,* 2014]. Nonetheless, the current knickpoint identification process is tedious and introduces a degree of subjectivity whenever the analyst visually defines a knickpoint. Selections can vary among different analysts or internally if analysts are inconsistent with their knickpoint selection criteria. Moreover, these techniques typically provide no consistent principle by which to define knickpoint dimensions, such as height, length, or slope.

To streamline knickpoint identification and measurement, we developed an algorithm that uses set criteria to objectively extract knickpoints from a DEM and measure various geometrical attributes pertaining to each knickpoint. These tasks are preformed automatically and largely independent of human bias or error. Recently, similar algorithms have been developed to identify knickpoints [*Gonga-Saholiariliva et al.,* 2011*; Queiroz et al.,* 2015], but these approaches do not include a means to automatically compare agreement between algorithm-selected knickpoints and a calibration dataset input by the user. Also, these existing algorithms generally do not make the suite of measurements needed to address spatial changes in knickpoint morphology. Here, the algorithm we develop quickly identifies knickpoints and measures knickpoint dimensions such as height, length, and slope. Using this approach, we demonstrate the effectiveness of an algorithm in rapidly identifying knickpoints and allowing for quick contextualization of different knickpoints types. This

rules-based approach improves the means of determining knickpoint origin, facilitates measurement of knickpoint geometries, and enables compilation of large knickpoint datasets that can be coupled with a regional slope map to map transience in a landscape. Comparisons can be made between the position of knickpoints and trends in knickpoint geometry, substrate lithology, tectonic structure, relative age, and hillslope gradient in order to assess patterns in knickpoint retreat.

Study Area

Santa Cruz Island (SCI) serves as a template to test and explore the effectiveness of our algorithm. Located ~36 km west of Ventura, Santa Cruz Island is the largest of the California Channel Islands (~250 km^2). The island displays features commonly associated with knickpoints (coastal terraces, steep hillslopes with debris flows and landslides, and hanging valleys). Additionally, the island contains diverse bedrock lithologies and has minimal infrastructure which could affect stream networks. Importantly, a 1-m-resolution LiDAR DEM enables detailed analysis of channel networks and hillslopes. Also, to analyze the effectiveness of the algorithm on various DEM resolutions, this DEM can be compared to a 10-m-resolution USGS national elevation dataset (NED).

Few studies have described the tectonic geomorphology and particularly the fluvial geomorphology on SCI [Patterson, 1977; *Sorlien,* 1994*; Pinter et al.,* 1998a*; Pinter et al.,* 1998b]. Moreover, these studies preceded the availability of high-resolution DEMs. This new DEM provides an opportunity to view this landscape through a new lens, and specifically, allows us to verify the effectiveness of a knickpoint selection algorithm, because many knickpoints (after initially located) are clearly visible on a 1-m-resolution elevation grid.

A. Vertical Tectonics

Santa Cruz Island (SCI), and the other neighboring Channel Islands, are interpreted to be the western surface expression of a blind, listric thrust fault that accommodated on the order of 3-5 km of contraction underneath the Santa Barbara Channel since the late Pliocene [*Pinter et al.,* 2003*; Seeber and Sorlein,* 2000]. An alternate fault bend fold geometry is proposed by Shaw and Suppe [1994] and suggests a larger amount of shortening: ~16 km over the same time period along low angle detachment faults. Although debate remains about which model most accurately estimates contraction through the Santa Barbara Channel, geomorphic markers suggest that vertical tectonics on the island have slowed considerably throughout the late Pleistocene. Three solitary corals on the lowest terrace level on SCI were dated using uranium-thorium series techniques [*Pinter et al.,* 1998a]. These ages display modest scatter, ranging from 124.8±1.4 ka to 135±2.3. Pinter et al. [1998a] report that this scatter could result from samples with enriched $^{234}U/^{238}U$ ratios relative to modern sea-water, suggesting that these ages may overestimate their true age by 0-20ka. With that caveat, these results were interpreted to reflect isotope stage 5e ages [*Pinter et al.,* 1998a], such that they suggest an uplift rate of ~0±0.1 mm/yr, depending on the elevation of the terrace platform. This assessment is supported by the observation of well-developed soils on the presumed stage 5e terrace on the southern coast of SCI *(Chadwick, personal communication)*. The uplift rate calculated for the lower terrace has been used in combination with the global δO18/ δO16 marine isotope sea level curve to crudely infer ages for older terrace platforms at higher elevations [*Pinter et al.,* 1998a, *Pinter et al.,* 1998b]: T2, T3, and Eastern-Terraces (Fig. 4). The uplift rate on SCI is strikingly slower than uplift rates measured from coastal terraces across the Santa Barbara Channel on mainland California (~0.75mm/yr - > 5 mm/yr since the last interglacial) [*Rockwell et al.,* 1992*; Trecker et al.,* 1998*; Gurrola et al.,* 2014].

A separate dating study conducted on submerged LGM paleoshorelines off the southern coast of SCI calculated uplift rates of 1.5±0.59 mm/yr based on radiocarbon dates of shoreline gastropods [*Chaytor et al,* 2008]; however, the elevation of these submerged paleoshorelines were compared LGM shoreline position estimates from sea level curves constructed in equatorial regions [*Lambeck et al.* 2002]. When considering LGM shoreline elevation corrected for local glacial isostatic adjustments affecting Southern California [*Muhs et al.,* 2012] the submerged LGM shoreline elevations dated by Chaytor et al. [2008], suggest subsidence on the order of 0.1 mm/yr.

Six more uplift-rate calculations based on dates of solitary coral fossils recovered from a seemingly correlative, broad, lower-terrace level of neighboring Santa Rosa Island and San Miguel Island reveal similarly low uplift rates [*Muhs et al.,* 2014]. The lower terrace level on both of these islands was dated to isotope stage 5e, yielding an uplift rate <0.2 mm/yr, supporting the findings of Pinter et al. [1998a] and interpretations that vertical tectonics have slowed considerably across the Channel Islands throughout the late Pleistocene [*Pinter et al.,* 1998a*; Pinter et al.,* 2001*; Muhs et al.,* 2014].

B. Bedrock Geology and Strike Slip Tectonics

Overall, the dominant lithologic groups on SCI are divided by the Santa Cruz Island Fault (SCIF). The SCIF is a left-lateral, strike slip fault and has been active in the late Pleistocene as shown by the left-lateral deflection of traversing steams and shallow trenching studies [*Patterson,* 1979; *Pinter et al.,* 1998b*; Pinter et al.,* 1998a]. The fault has a horizontal slip rate of approximately 0.8 mm/yr and a smaller vertical component of around 0.1 mm/yr (north side up) determined from offset of the stage 5e terrace [*Pinter et al.,* 1998a].

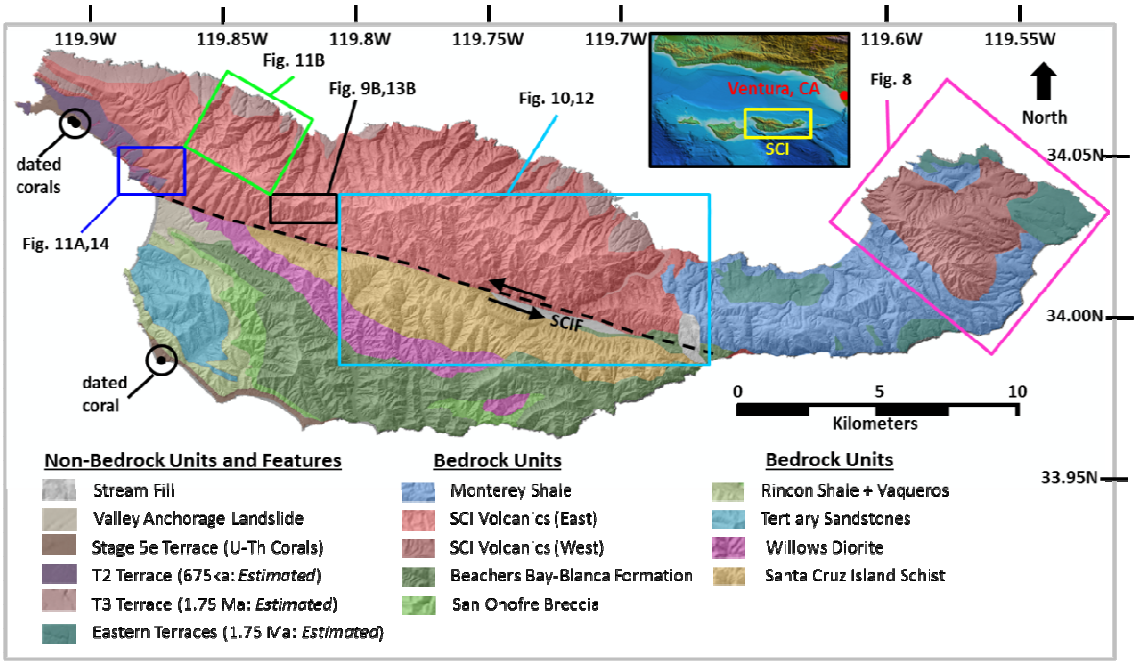

Figure 4) Geologic map of Santa Cruz Island, after *Weaver and Nolf* [1969]*; Dibblee Jr.* [1991]

Bedrock north of the SCIF consists of andesitic flows and volcaniclastic rocks (Santa Cruz Island Volcanics) that overlie the Monterey Shale on the northeast portion of the island [*Nolf and Nolf,* 1969]. The volcanic rocks form a prominent ridge including the highest peaks on the island and are considered to be some of the most resistant rocks on the island [*Weaver and Meyer,* 1969]. South of the SCI Fault, rock units span lower Tertiary sandstones and siltstones, more competent Miocene Blanca and San Onofre conglomerates, heavily weathered Precambrian SCI schist, and Jurassic Diorite [*Weaver and Nolf,* 1969*; Dibblee Jr,* 1991]. Most of the high peaks (~400 m) in the southern part of SCI are underlain by Sierra Blanca conglomerates and Willows diorite; however, these peaks are approximately half the elevation of the peaks in the northern SCI volcanic rocks (~800 m). The lower Tertiary sandstones and siltstones are confined to the southeast corner of the island and are notably weak, exhibiting gully erosion, friable outcrops, and widespread arroyoing [*Perroy et al.,* 2010].

II. *Methods*

A. *Algorithm Construction*

The knickpoint selection algorithm uses applications of topotoolbox software [*Schwanghart and Scherler,* 2014] and a stream-power based chi-plot visualization of landscape evolution. A brief review of the chi-plot representation of a landscape is presented below along with an explanation of why this representation is useful in automated knickpoint selection.

A chi plot is constructed by integrating a landscape-evolution shear-stress incision-based model:

$$dz/dt = U(x,t) - K(x,t)A(x,t)^m|dz/dx|^n \qquad \textit{Equation 1}$$

where: z = elevation, t = time, x = longitudinal position along a stream profile, U = uplift rate, K = constant which considers rock strength and climatic factors, A = upstream drainage area, m = a constant relating drainage area to discharge and catchment geometry, and n = a constant relating channel slope to erosional efficiency [*Howard and Kerby,* 1983*; Whipple and Tucker,* 1999]

Under a steady-state assumption, dz/dt = 0, and this relationship simplifies to:

$$|dz/dx| = (U(x,t)/K(x,t))^{1/n}A(x,t)^{-m/n} \qquad \textit{Equation 2}$$

$$\text{or } S = k_s A^{-\theta} \qquad \textit{Equation 3}$$

where: S = local channel slope, $k_s = (U(x,t)/K(x,t))^{1/n}$, and $\theta = m/n$

In a case when U(x,t) and K(x,t) are constant, Eq. 3 plots as a negatively sloping line in log(S)/log(A) space, with the y intercept of k_s (channel steepness), and a slope of -θ (channel concavity) (Fig. 5B). Variations in channel steepness and channel concavity from stream to stream or within one stream have been useful in identifying spatial changes in uplift rate, erosion rate, and channel adjustment through knickpoint propagation [*Kirby and Whipple,*

2001*; Synder et al.,* 2000*; Wobus et al,* 2006a*; DiBiase et al.,* 2010*; Kirby and Whipple,* 2012].

Alternatively, channel steepness and concavity can be visualized and calculated by integrating Eq. 2 with respect to incremental changes in drainage area as a function of changing position upstream (see Perron and Royden [2013] for full derivation):

$$Z(x) = z(x_b) + (U/K*A_0^m)^{1/n}\,\chi \qquad \textit{Equation 4}$$

Where the variable 'chi' (χ) $= \int_{xb}^{x} (A_0/A(x))^{m/n} dx$ *Equation 5*

x_b = "x" position of baselevel, $z(x_b)$ = elevation at baselevel, A_0 = a reference drainage area used to compare relative changes in drainage area [*Perron and Royden,* 2013].

Again, with a constant U(x,t) and K(x,t), Eq. 3 will plot as a line in elevation/chi space, with $z(x_b)$ as the y-intercept and $(U/K*A_0^m)^{1/n}$ as the slope of the line for increasing χ. Note that $(U/K*A_0^m)^{1/n} = k_s/(A_0^m)^{1/n}$ and that $(A_0^m)^{1/n}$ = an arbitrary constant. Hence, the slope of the line in elevation/chi space represents the stream steepness (k_s) (Fig. 5). Using this approach, the channel concavity can be derived using a Monte Carlo analysis that loops through a range of possible channel concavities and identifies which concavity best linearizes the elevation/chi curve. See Perron and Royden [2013] for a complete list of advantages and disadvantages within the chi-plot representation of a stream profile.

Log-slope/log-area plots also have an expected linear trend when analyzing a well-adjusted, graded stream, but because drainage area is the dependent variable in this type of representation, gaps form between adjacent data nodes where confluences of large tributaries create stepwise increases in drainage area [*Perron and Royden,* 2013]. Furthermore, noisy topographic slope data calculated from a DEM usually requires a degree of smoothing or log-binning of data. The dependent variable chi can be calculated through Eq. 5 at equally spaced nodes at the resolution of a DEM, a procedure that reduces gaps at tributary

confluences and eliminates noise that would result from differentiating across a topographic surface to calculate local slope (Fig. 5).

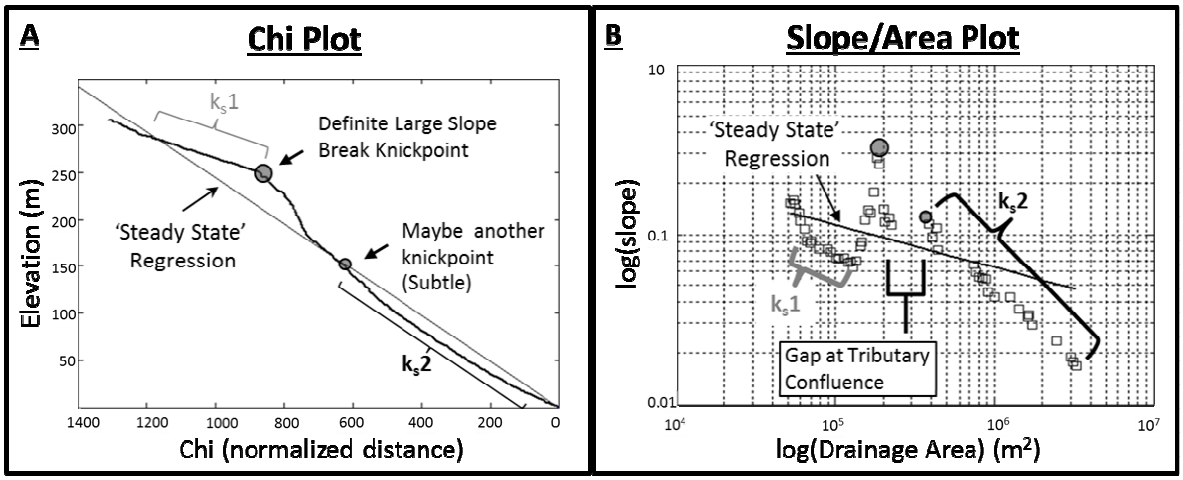

Figure 5) Chi plot and slope-area plot of the same stream containing a large slope-break knickpoint and a possibly a more subtle knickpoint downstream. A) The chi plot expresses knickpoints as regions where the plot changes slope, (where an increase in k_s, stream steepness index, occurs). The change in k_s can be maintained throughout the downstream length of the profile (slope-break knickpoint) or be localized (vertical step knickpoint). B) In the slope area plot, knickpoints are expressed as regions with anomalously high slopes for a respective drainage area (again high k_s). Notice that the slope area plot contains stepwise jumps in drainage that occur at tributary confluences which create cause gaps between plotted data points. One of these gaps falls near the location of a potential knickpoint and could cause this feature to go unnoticed if only a slope area plot was used to visualize this landscape. Also, note that each data point in the slope area plot represents the median of 100 log-binned slope measurements.

For automated knickpoint selection, the largest advantage of using a chi-plot representation is the removal of a stream's natural concavity that results from an exponential increase in drainage area as position moves downstream [*Hack,* 1957]. A well-adjusted, ideal graded stream will plot as a concave-up curve in elevation-distance space [*Flint,* 1974]; however, in elevation-chi space, the same stream will plot as a straight line, because the variable chi encompasses progressive changes in upstream drainage area normalized for changes in upstream distance (Fig. 6).

Our algorithm utilizes the continuous record and expected linear trend of a "steady-state" longitudinal chi plot. These factors allow for a simple de-trending of stream profiles relative

to a linear best-fit regression (Fig. 6). The regression represents a steady-state, theoretical stream spanning the chi bounds of the surveyed stream, but functioning in accordance to "ideal" conditions: uniform temporal and spatial uplift, sediment flux/caliber, precipitation/runoff fraction, and substrate resistivity [*Kirby and Whipple,* 2001*; Sklar and Dietrich,* 2001*; Duvall et al.,* 2004*; Dibiase and Whipple,* 2011*; Perron and Royden,* 2013]. The residual between a stream's chi profile and a linear regression (a "de-trended" chi plot) represents the deviation from an idealized, uniform stream. Such plots express where a stream is "understeepened" or "oversteepened" with respect to steepness of the theoretical ideal longitudinal profile (Fig. 6C).

Local maxima in a de-trended chi plot represent potential knickpoint lips where the stream is at a local maximum elevation relative the best-fit linear regression, and local minima represent potential knickpoint bases where the stream profile is at a local minimum elevation relative to the best-fit linear regression. These two points delineate the bounds of a knickpoint (Fig. 6B-C). Importantly, the elevation loss across the knickpoint interval can be readily determined. The difference between (i) the observed elevation loss between the bounds of the knickpoint and (ii) the loss expected by the best-fit regression for the profile defines the "magnitude" of the knickpoint. Additionally, the horizontal distance between the knickpoint bounds yields a knickpoint length that can be used to calculate a knickpoint

slope.

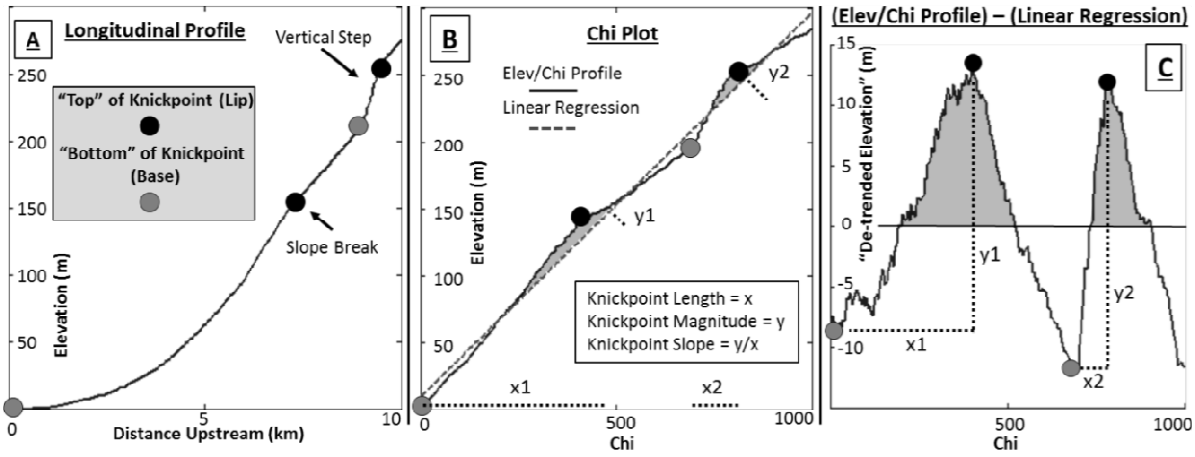

Figure 6) A) Longitudinal stream profile exhibiting a slope-break knickpoint and a vertical step knickpoint. B) A transformation of stream longitudinal profile into "chi" space. This plot displays the same data, but with the natural concavity of the stream removed. Now the stream profile can be compared to a linear best-fit regression. C) A "De-trended" chi plot represents the elevation residual between the chi profile and the linear best-fit regression, such that knickpoint lips plot as local maxima, and knickpoint bases plot as local minima. Insignificant convexites resulting from topographic noise can be removed using a Savitzk- Golay smoothing filter and setting a minimum knickpoint magnitude (y) condition.

Complications arise when measuring slope-break knickpoints that exist as discrete points (Fig. 1B). These knickpoints only have a lip coordinate and no base; the magnitude and length of these knickpoints is calculated by comparing the position of the lip coordinate to the position of the mouth of the stream or confluence. Although the magnitude of the knickpoint will yield a different elevation change than what would be calculated from extrapolating a relict longitudinal profile on the basis of its upstream concavity [*Clark et al.,* 2005; *Harkins et al.,* 2007*; Kirby and Whipple,* 2012*; Dibiase et al.,* 2014] , this measurement still characterizes the relative amount of elevation loss accrued through the slope-break knickpoint and is useful in comparing the relative size of multiple knickpoints scattered through a landscape.

A degree of smoothing is required to remove small convexities in stream longitudinal profiles that result from DEM artifacts or small bedrock steps that are smaller than the scale

of knickpoint analysis. For the interested reader, refer to the supplementary information which details these smoothing processes (Supplementary Fig. 4-5). Importantly, these smoothing functions can be adjusted to fit the scale of analysis or the resolution of the DEM. The knickpoint selection algorithm includes a calibration function where the user can input known, or hand-selected knickpoint positions (e.g. using techniques from *Wobus et al.,* [2006a]), and compare these positions to the algorithm outputs for various smoothing parameter combinations (Supplementary Fig. 6). This feature allows the analyst to quickly tune parameters to fit the goals of their analysis.

B. *DEM Preparation and Analytical Methods*

The knickpoint-selecting algorithm was applied to catchments on Santa Cruz Island (SCI) with a drainage area > 1 km^2. A minimum drainage area of 50,000 m^2 was used to define the break between hillslope-colluvial reaches and fluvial channels [*Montgomery and Foufoula-Georgiou,* 1993]. The 1-m resolution of the DEM permits use of a relatively low minimum drainage area and slope-area plots confirm that 50,000 m^2 typically marks the transition to a linear decreasing log-slope/log-area relationship in SCI catchments (Fig. 5).

Knickpoint-selection smoothing parameters were determined by maximizing agreement with calibration knickpoints selected individually, using techniques outlined by *Wobus et al., 2006a* (Supplementary Fig. 6). A Savitzky-Golay [1967] smoothing window of 225 cells, a lumping window of 125 chi, and a minimum knickpoint size of 3 m was found to best replicate calibration knickpoint size and position for the 1-m resolution LiDAR DEM.

The same procedure was applied to a 10-m resolution DEM of the largest catchment of SCI to compare the effectiveness of the algorithm on multiple DEM resolutions; however, the minimum drainage area was increased to 100,000 m^2, and the Savitzky-Golay smoothing

window was reduced to 21 cells to scale with the lower DEM resolution. The results of this comparison are included in the supplementary text (Supplementary Fig. 8).

A field survey was performed to verify the accuracy of knickpoints selected by the algorithm (Supplementary Fig. 7). Field verification was limited to streams crossing the coastal terrace on the northwestern portion of the island, because the majority of other knickpoints were located in steep, inaccessible terrain. In these regions, all but one of the knickpoints located by the algorithm were verified in the field and exhibited heights comparable to the knickpoint magnitude measured by the algorithm. The unverified knickpoint was likely misidentified in the field at a drainage area less than the 50,000 m^2.

Due to the large file size of the 1-m DEM, the knickpoint selection algorithm was applied to 4 provinces, clipped from the full SCI-DEM. These provinces were distinguished based on weathering characteristics likely representative of bedrock lithology characteristics: 1) volcanic rocks of northern SCI, 2) Monterey Shale, 3) weak Tertiary sandstones of southwestern SCI, and 4) more competent conglomerates, schist, and diorite of southern SCI. Each classification displays a different topographic expression visible on the LiDAR imagery, namely relief and maximum elevation (Fig. 7). Additionally, this division allows us to characterize differences between knickpoint behavior in streams traversing varying lithologies.

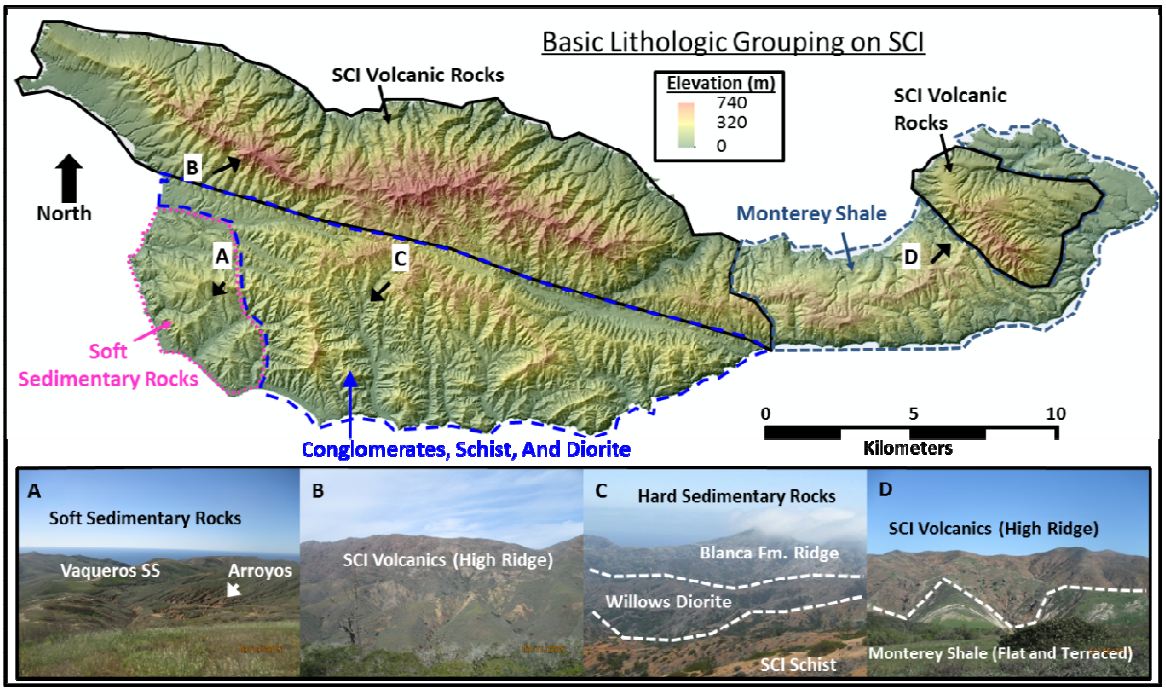

Figure 7) Provinces on SCI selected by dominant lithologies and weathering characteristics: arrows on map show the view aspect for field photographs. High ridges are supported in northern SCI by volcanic rocks and in southern SCI by Blanca Fm. conglomerates and SCI schist.

III. *Results*

Using the parameters specified in the previous section, we located 808 knickpoints on Santa Cruz Island with magnitudes ranging from 3 m and 83 m of de-trended elevation drop (drop in elevation not explained by the average steepness of the river Fig. 6). Given their spatial context, certain knickpoints show convincing evidence for both migratory (externally sourced) and fixed (internally sourced) knickpoints (Figs. 2 and 3). A complete map plotting the position of all of the knickpoints located in this study is included in the supplementary materials (Supplementary Fig. 1); this results section focuses only on specific examples of knickpoints with relatively clear origins.

A. Fixed (internally sourced) knickpoints

Knickpoints with spatial consistency along the geologic contact between Monterey Shale and SCI Volcanics highlight an inferred change in substrate erodability from volcanic

to shale bedrock (Fig. 8). Presumably, the more resistant volcanic rocks support higher, steeper topography adjacent to the Monterey shale which lies relatively flat at lower elevations (Fig. 7-8); this contrast generates a topographic step between the two units. Knickpoints siting along this step would likely be stationary features, fixed to the geologic contact between the two units [*Wobus et al.,* 2006a*; Burbank and Anderson,* 2011]. Yet, even given the spatial consistency of these knickpoints on the geologic contact, possibility remains that a component of these knickpoints' elevation-drop resulted from a base-level signal that has migrated upstream but stalled on this geologic contact due to the transition from soft to hard bedrock.

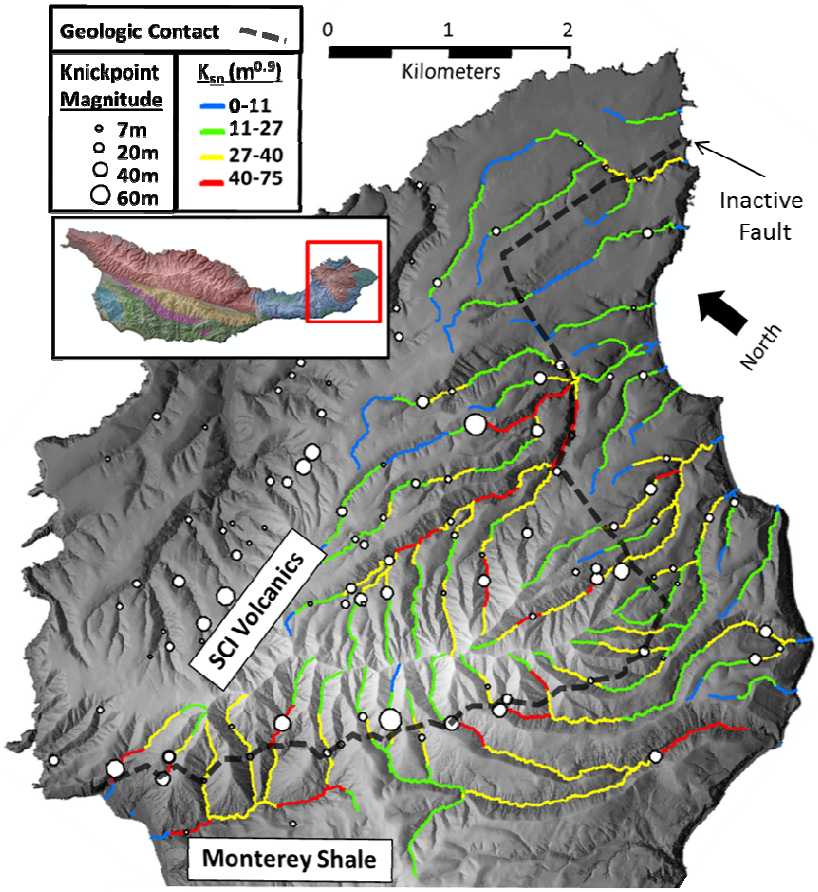

Figure 8) Spatial map of knickpoints in eastern SCI reveals correlation between knickpoint position, k_{sn} and the mapped geological contact between SCI Volcanics and Monterey Shale. Knickpoints are situated consistently along the geologic contact and exhibit generally higher k_{sn} values only locally in these positions (vertical step knickpoint).

Within sections of SCI Volcanic bedrock, knickpoints are closely associated with specific protruding beds that appear to be significantly more resistant to erosion than surrounding rock. The resolution of the LiDAR imagery allows us to trace these beds laterally and see knickpoints fixed to these steps (Fig. 9). Importantly, some of these knickpoints have a considerable magnitude (>20 m). In the absence of high resolution imagery, such knickpoints might be interpreted as migratory features because they do not appear fixed to a mapped geologic contact (all bedrock within this region is mapped as SCI Volcanics). Again, k_{sn} generally increases through stream segments where resistant beds support knickpoints but exhibits lower values upstream and downstream from these locations. K_{sn} measurements were calculated at intervals of 200 m, so resolution of these measurements is too coarse to identify the effects of individual resistant beds on stream steepness. Also, these knickpoints occur at relatively low drainage areas for fluvial slope-area analysis (~100,000 m^2). The low discharge and sediment flux at these positions in the stream network could enhance the ability of these resistant beds in supporting knickpoints

[*Crosby and Whipple,* 2006; *Wobus et al.,* 2006b].

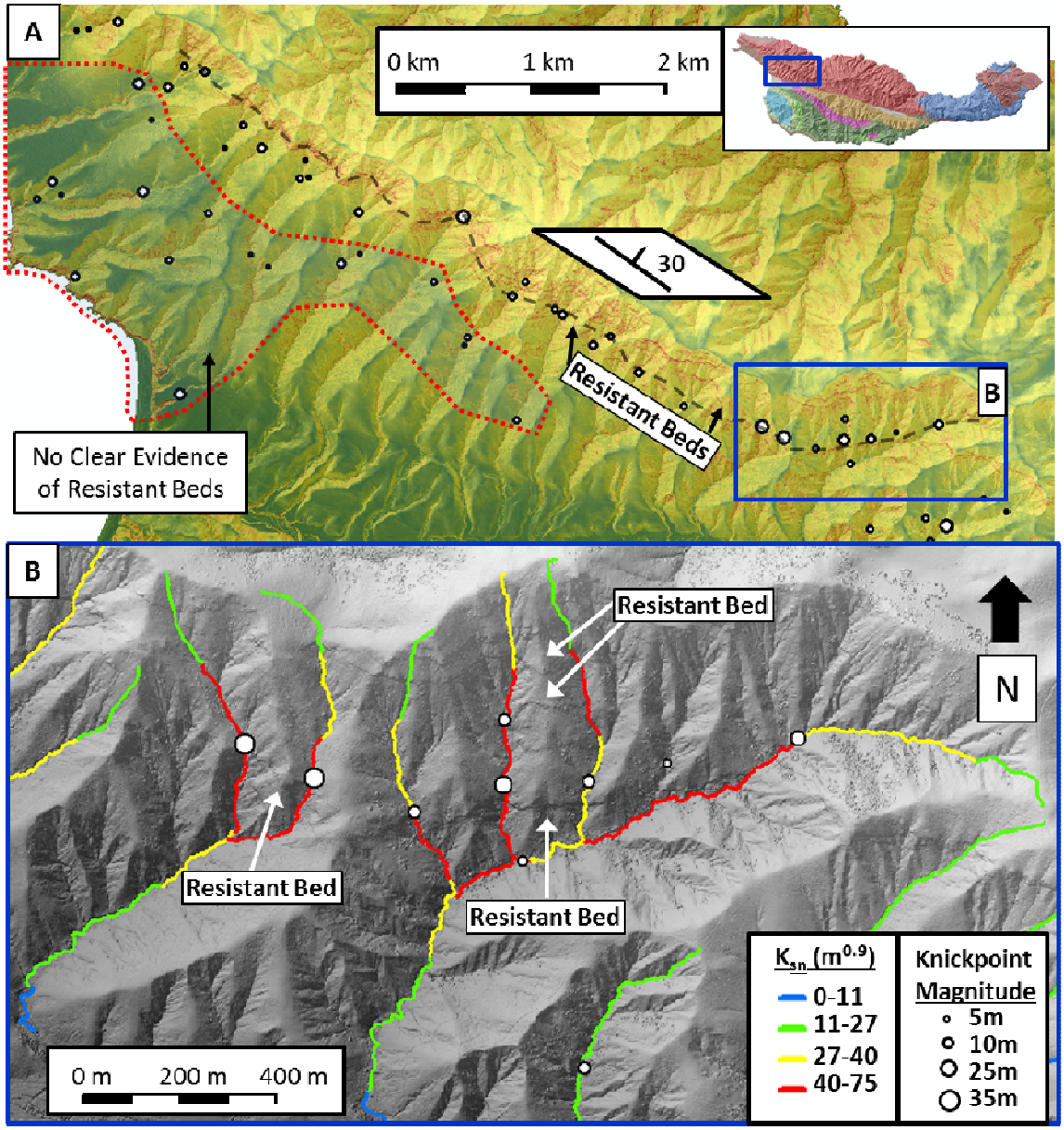

Figure 9) A) Knickpoints fixed to resistant beds within volcanic units in the northern portion of SCI. Resistant beds are visible as orange-red lines that follow the measured strike and dip in this region (one prominent bed is highlighted with a black, dashed line). B) Blow up of region containing larger knickpoints fixed to prominent beds. k_{sn} is high only in regions spanning the resistant beds suggesting that these knickpoints are relatively fixed to their current location. None of these knickpoints fall on a mapped geologic contact.

B. *Migratory Knickpoints: Stream Capture and Incision*

The largest catchment draining the central valley of SCI into Prisoner's Harbor Clear exhibits an interpreted migratory knickpoint signal, radiating throughout the catchment with little relationship to bedrock lithology (Fig. 10B, red dotted line). Using the distribution of these knickpoints and the unusual shape of the central valley catchment, we infer that a stream capture event generated this transient knickpoint signal (see Fig. 10, A and B). Stream capture events have been noted to initiate rapid channel incision and waves of migratory knickpoints throughout catchments in relatively quiescent or steady-state tectonic environments [*Tinkler et al.,* 1994; *Hasbargen and Paola,* 2001; *Prince et al.,* 2011].

The current drainage pattern of the central valley stream empties into Prisoner's Harbor on the northeast shore of SCI (Fig. 10B); however, an elevation profile taken through the central valley (which parallels the SCI Fault running towards Valley Anchorage) shows remnants of a previously graded stream profile that connects the relict channel upstream of the trunkstream knickpoint to the present-day catchment divide in the eastern edge of the central valley (Fig. 10, A and C). The fit of this reconstruction and the unusual shape of this catchment indicate that flow likely originally drained southeast along the SCI Fault to Valley Anchorage and was captured by a northward draining stream which had a more direct route to baselevel fluctuations possibly initiating headward retreat into the central valley. The stream-capture established the current channel network that now drains northeast through a narrow canyon and empties into Prisoner's Harbor.

Step-wise addition of the central valley drainage area would have drastically increased the erosive power of the northward draining, capturing stream. This pulse in stream power presumably would have rapidly accelerated down-cutting through the ~100 m coastal terrace which spans the northern coast of SCI. This stream is the only stream on the northern coast which has effectively incised through the entire height of the coastal terrace; all other

streams draining to the northern coast exhibit knickpoints near the mouths of their streams (Supplementary Fig. 1). The pulse of incision through the coastal terrace has been transmitted upstream through a large trunkstream knickpoint (~100 m), generating similarly sized knickpoints in tributaries adjusting to the new baselevel downstream from the trunkstream knickpoint (Fig. 10, B and D). The height of these knickpoints in the tributaries is roughly consistent with their elevation plotted on the reconstructed, pre-capture profile, with some of the knickpoints in larger tributaries migrating some distance upstream from their likely elevation of origin (Fig. 10, C and D).

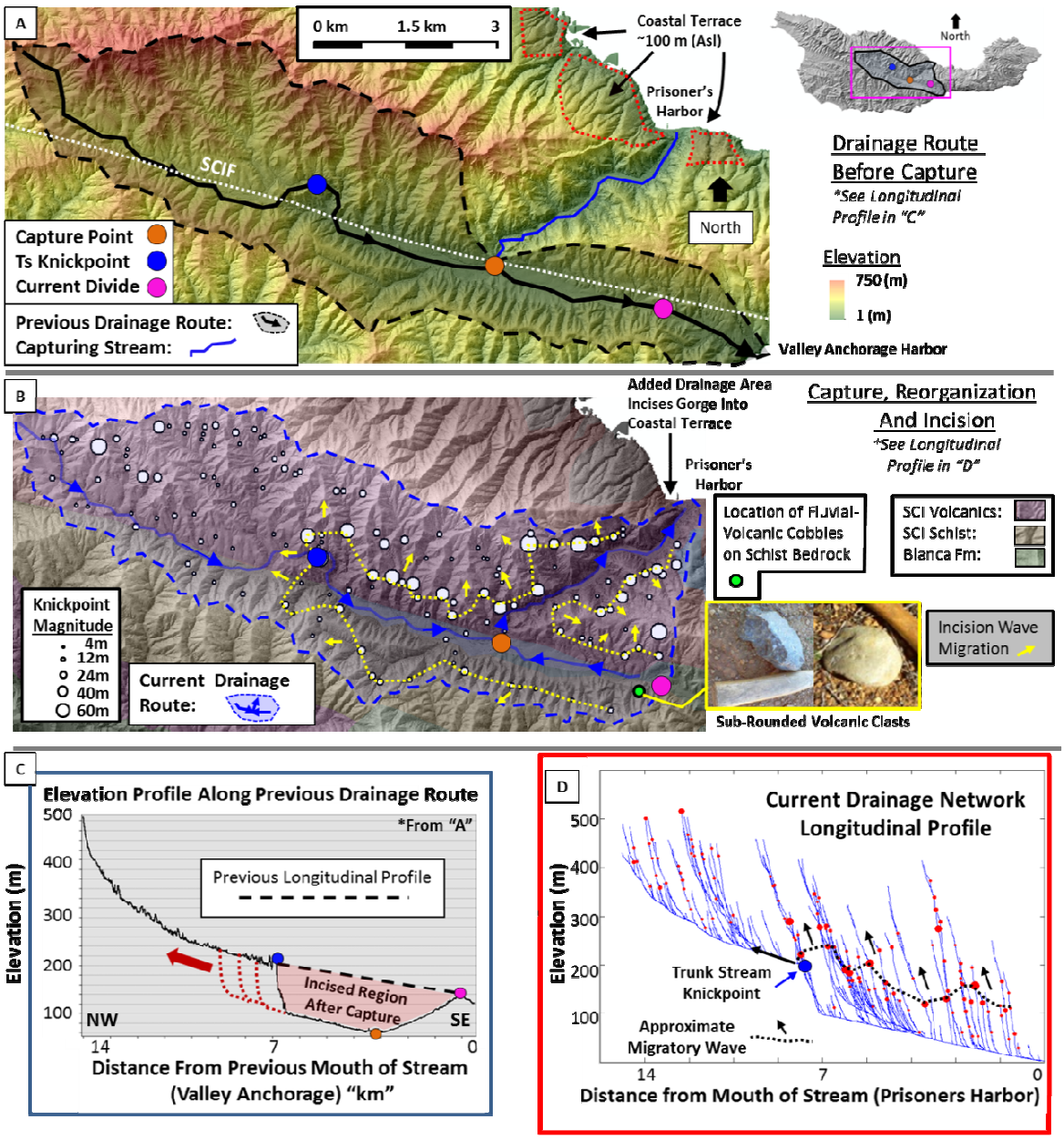

Figure 10) A) Inferred previous drainage pattern based on the current catchment shape, subdued southeastern catchment divide elevation, and well-graded, reconstructed longitudinal profile (in C). B) Current drainage network and catchment shape displaying radially distributed large knickpoints, a northward-draining stream appears to have captured the drainage area of the central valley and diverted drainage northward to Prisoners Harbor (rather than towards Valley Anchorage). C) Reconstructed longitudinal profile taken from an elevation transect along the black solid line in A. Noise in the longitudinal profile is a result of channel roughness and channel meanders around the transect line (from "A"). D) Knickpoints in tributaries and the main stem have migrated upstream as a result of stream capture and base-level lowering through the coastal terrace.

Alternatively, one could suggest that the SCI strike-slip fault (SCIF) running through the central valley has a more significant vertical-slip component in this location (Fig. 10A),

leading to knickpoint generation in streams flowing from the up-thrown side (north); however, this fault trends through the entire catchment, and large knickpoints are mostly confined to only the downstream, eastern part of the central valley. If there has been significant vertical slip along the SCIF, there would be some expression of this motion in the western portion of the catchment unless deformation is highly localized in the eastern side of the central valley. If vertical motion on the SCIF has been concentrated in the eastern central valley where the large knickpoints are present, a higher range-crest elevation might also be expected in this area [*Stein et al.,* 1988]. Instead, the range crest north of the SCIF has a consistent peak elevation between 550 and 650 m (Fig. 10A). These observations provide little evidence for accentuated vertical throw on the SCI fault in the regions where streams exhibit large knickpoints. Consequently, stream capture and incision remain the most likely explanations for the generation of these large knickpoints.

Provenance evidence provides further support for the stream capture hypothesis. Sub-rounded volcanic clasts were recovered from an interfluve in the easternmost portion of the central valley near the current divide where today's streams are flowing west toward the hypothesized point of capture (Fig. 10B). With today's drainage configuration, this interfluve only derives material from upstream slopes with SCI schist bedrock. The closest source for the volcanic clasts lies to the northwest and transport to their current location would require a drainage network similar to our hypothesized pre-capture configuration (Fig. 10A).

C. Migratory (externally forced) Knickpoints: Coastal processes

Numerous knickpoints are situated at the mouth of coastal streams, seemingly correlative to diverse marine terrace platform levels around the island (Fig.11 and Supplementary Fig. 1). Scenarios where obvious, rapid, large-magnitude relative sea-level fall events have

produced coastal knickpoints serve as useful case studies to analyze landscape response time [*Loget et al.,* 2009], modes of knickpoint migration [*Bishop et al.,* 2005; *Jansen et al.,* 2011; *Castillo et al., 2013*], and in turn, could potentially be used to assess the timing of relative sea-level changes. Yet, interpretations of coastal knickpoints must be made with caution in many cases. In the absence of correlative, datable strath terraces [*e.g Seidl et al.,* 1997; *Mackey et al.,* 2014], the formation time of these knickpoints is often challenging to calculate in a landscape. Also, coastal knickpoints can reflect strong wave erosion of sea-cliffs or baselevel fall that occur at both sea-level high-stands and low-stands [see *Synder et al.,* 2002]; moreover, these knickpoints could possibly even stem from features now submerged under the current sea-level highstand. The spatially extensive map of knickpoints in coastal streams on SCI can be used to address some of these uncertainties with respect to the multiple terrace platforms that are preserved along the coast of SCI and vary from an age of ~125 ka to inferred ages of up to 1.75 Ma [*Pinter et al.,* 1998a; *Pinter et al.,* 1998b].

T2 (assumed age 675 ka – *Pinter et al.,* 1998a) and T3 (assumed age 1.75 ma – *Pinter et al., 1998a*) terrace platforms are extensively preserved along the northwestern coast of SCI (Fig. 4). Channels dissecting these terraces consistently exhibit two knickpoints: (1) an upstream knickpoint, above which the relict channel profile can be extended to grade to the position of landward extent of the T2 or T3 wave-cut platform, and (2) a downstream knickpoint which sits near the coast at an elevation below these terrace platforms (Fig. 11). The terrace platforms and longitudinal profiles upstream from these lower knickpoints can be projected seaward to an intersection point near present day sea-level. In an ideal case, the location of intersection between these lower stream profiles may represent the former coastline prior to sea-cliff retreat after establishment of the current sea-level highstand, ~4 ka

in California [*Nardin et al.,* 1981. If true, these reconstructions could be used to estimate longer term sea-cliff retreat rates and the mechanisms which these stream-channels use to adjust to this forcing. However, these reconstructions could easily oversimplify coastal processes and longitudinal profile form. Errors in these reconstructions may stem from drawdown reaches extending upstream from knickpoints [*Berlin and Anderson,* 2009], the presence of resistant beds that alter the geometry of a stream's longitudinal profile [*Marshall and Roering,* 2014], or the prior existence of now-submerged or undercut knickpoints from previous sea-level changes that a simple extrapolation would not capture.

More specific analyses with cosmogenic radionuclides would be needed to assess the timing of knickpoint formation or sea-cliff retreat rates and test the hypothesized scenario here (Fig. 11) [*e.g Seidl et al.,* 1997; *Mackey et al.,* 2014]. Yet, the consistency of these knickpoints in streams crossing various terrace levels suggests both relative sea-level fall and sea-cliff retreat exert a significant control on coastal stream profiles. The terrace-correlated, upper knickpoints have retreated noticeably further in the streams traversing the T3 platform, which is expected considering the T3 terrace is presumed twice as old as T2, and these streams traverse the same lithology, have a similar drainage area, and likely carry similar discharges and sediment fluxes.

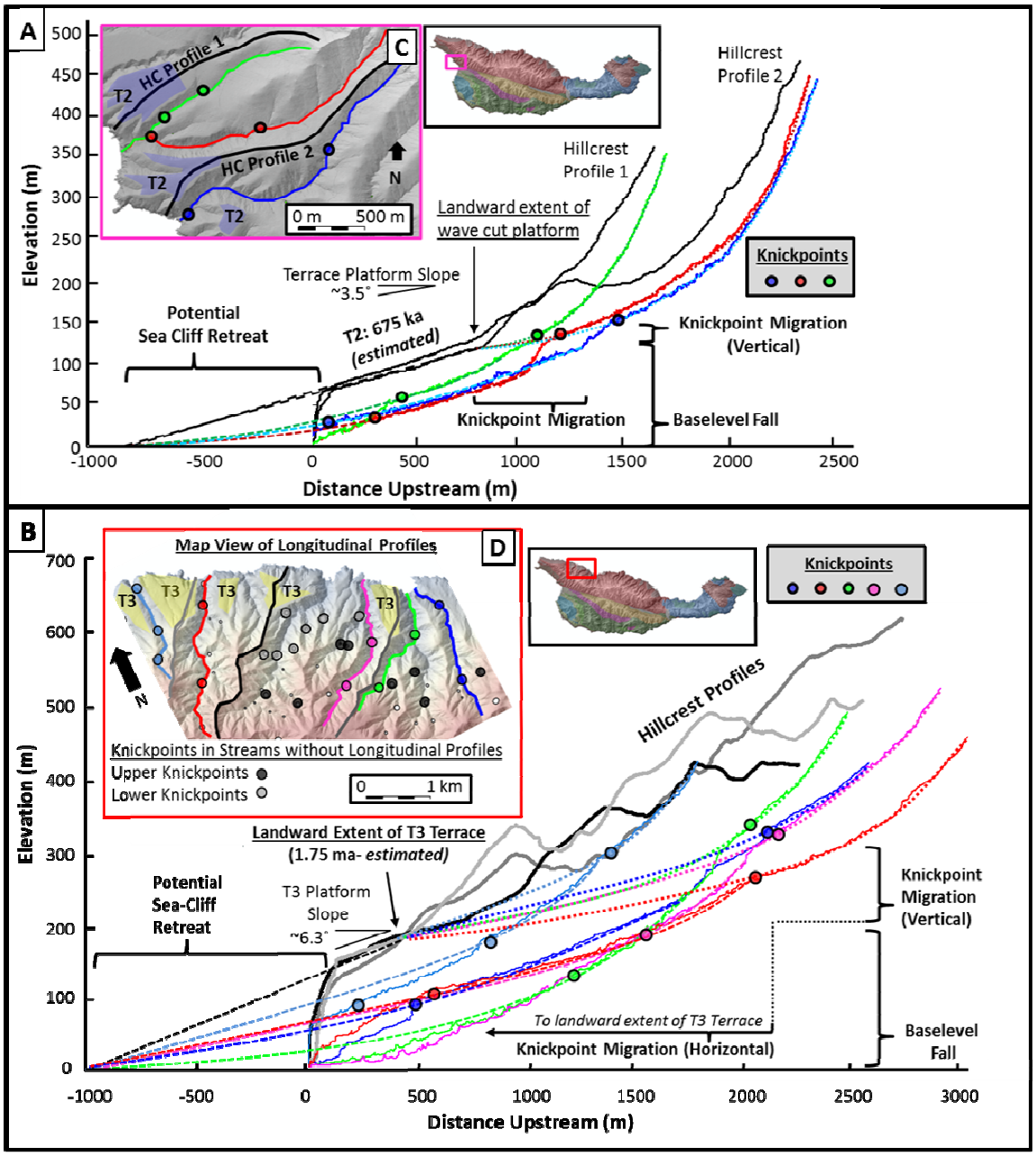

Figure 11) Detailed analysis of coastal streams and reconstructed longitudinal profiles. Hillcrest profiles (black-gray) record the landward extent of the wave-cut platform as break in slope from the gradual terrace platform to steeper stream interfluves. A) T2 terrace-dissecting stream profiles and reconstructions. B) T3 terrace-dissecting stream profiles and reconstructions. Longitudinal hillcrest and stream profiles are color-coordinated with their spatial position on the DEM (inset C and D). D) Additional streams display similar knickpoint distribution patterns with respect to the T3 terrace but do not fit on our longitudinal profile plot. Small knickpoints at high elevations and low drainage areas may reflect substrate heterogeneities or an expression of an even higher surface.

III. *Discussion*

Application of a new algorithm designed to find and quantify knickpoints reveals clear examples of knickpoints that are fixed to resistant portions in a landscape (Fig. 8-9) and knickpoints that are migrating upstream from base-level changes induced by stream capture, long-term coastal uplift, or sea-cliff retreat (Fig. 10-11). This diversity gives us the opportunity to quantitatively compare landscape morphologies surrounding both knickpoint types, and furthermore, suggest that specific differences in landscape morphology upstream and downstream from knickpoints can be used to assess knickpoint mobility.

Typically differentiation between migratory and fixed knickpoints is performed using a geologic map and comparing the spatial distribution of knickpoints to mapped geological contacts (Wobus et al., 2006; Miller et al., 2013). In some cases, this differentiation is sufficient (Fig. 8); however, in other cases, reasonably large magnitude (>20 m) knickpoints can be fixed to specific resistant beds embedded within a geologic unit and are not necessarily distributed along mapped contacts (Fig. 9). To distinguish these more stationary knickpoints from examples of significant transient knickpoints (Fig. 10-11), simple analyses can be performed on adjacent hillslopes to identify whether a landscape is likely: 1) in a steady state surrounding a fixed knickpoint or 2) in a transient state surrounding a migratory knickpoint.

A. *Using Hillslope Steepness to Distinguish Migratory and Fixed Knickpoints*

Under simple geometrical considerations, migratory knickpoints leave a path of oversteepened hillslopes downstream from their location as the stream channel lowers its elevation in a step-wise fashion, faster than the adjacent hillsopes [Gallen et al., 2011]. As well as being an indicator for knickpoint migration, these hillslopes are more prone to debris flows, landslides, and mass-wasting events [*Bigi et al.,* 2006; *Gallen et al.,* 2011; *Tsou et al.,* 2014], and may exist in this oversteepened form for some lag time on the order of 10^3 to 10^5

ky until hillslope processes re-adjust to the fallen local baselevel [*Hilley and Arrowsmith,* 2008]. Capitalizing on a 1-m resolution bare-earth DEM, we can quantify changes in hillslope steepness upstream and downstream from both presumably migratory and fixed knickpoints. Additionally, in steep terrain, the DEM resolution is sufficient to identify geomorphic markers of hillslope failures remotely using the imagery.

In the central valley of SCI where stream-capture related incision has produced large, radially-distributed knickpoints, a histogram of pixel-pixel slope distributions is calculated both upstream and downstream from the knickpoints. The pixel frequency for each slope interval in the histogram is normalized by the median slope interval. The median slope value portrays the most representative hillslope angle for each region.

Normalized Pixel Frequency for Slope Interval = Frequency in Bin/Frequency in Median Bin

Downstream from the knickpoints in the central valley, the median slope value is approximately 5˚ steeper than median slope value upstream from the knickpoints (Fig. 12). Moreover, 36.4% to 16.8% of the landscape downstream from the knickpoints exhibit slopes that exceed threshold values of 35 to 40˚, as opposed to only 21.7%-9.1% of the landscape upstream from the knickpoints (Supplementary Fig. 3) [*Carson and Petley*, 1970; *Schmidt and Montgomery,* 1995; *Burbank et al.,* 1996; *Montgomery and Brandon*, 2002; *Dibiase et al.,* 2012]. Zooming in on some of the larger knickpoints, streams exhibit even more profound differences in hillslope gradient upstream and downstream from larger knickpoints

(Fig. 13A,C).

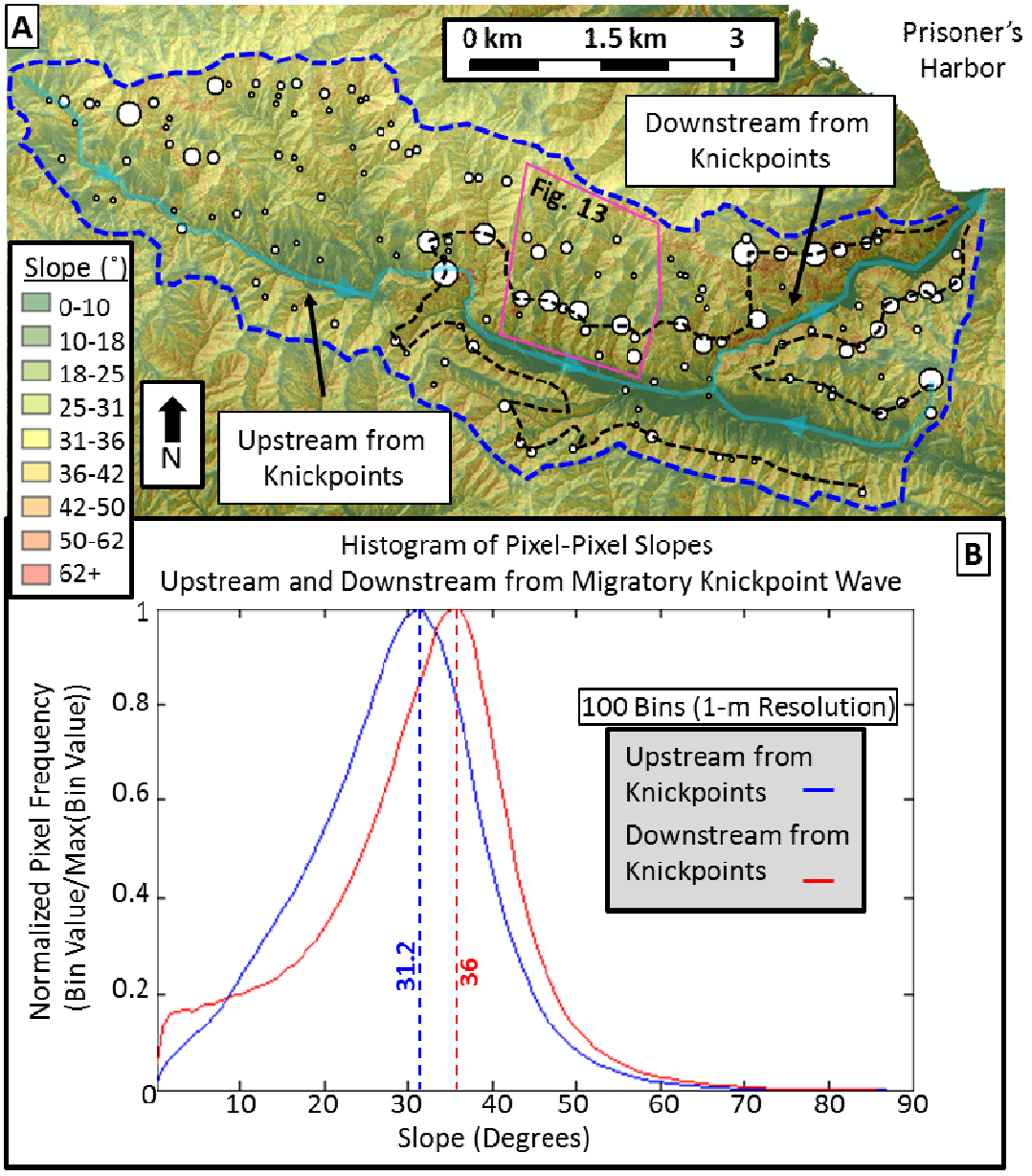

Figure 12 A) A regional slope map displays the spatial distribution of pixel-pixel slope values calculated on a 1-m DEM. The black-dashed line that runs through the large magnitude knickpoints approximates the division between relict and adjusted topography. B) Distribution of slope values upstream from the black-dashed, knickpoint line and downstream from the black-dashed, knickpoint line. The adjusting landscape downstream from the knickpoints is approximately 5˚ steeper than the relict topography upstream from the knickpoints.

Slope distributions are nearly identical upstream and downstream from knickpoints that appear fixed to resistant beds or geologic contacts (Fig. 13B-D, Supplementary Fig. 2). This

continuity suggests that the landscape is in a near steady-state with protruding resistant beds that support localized knickpoints. The hillslopes have graded to the position of the stream and are not forced to adjust to migrating knickpoints. Additionally, the resistant beds can be traced laterally and steepen the interfluves between neighboring catchments (Fig. 13B), whereas downstream from the migratory knickpoints the interfluves express low gradients, with the steepened hillslopes confined between the ridge top and stream bottom (Fig. 13A).

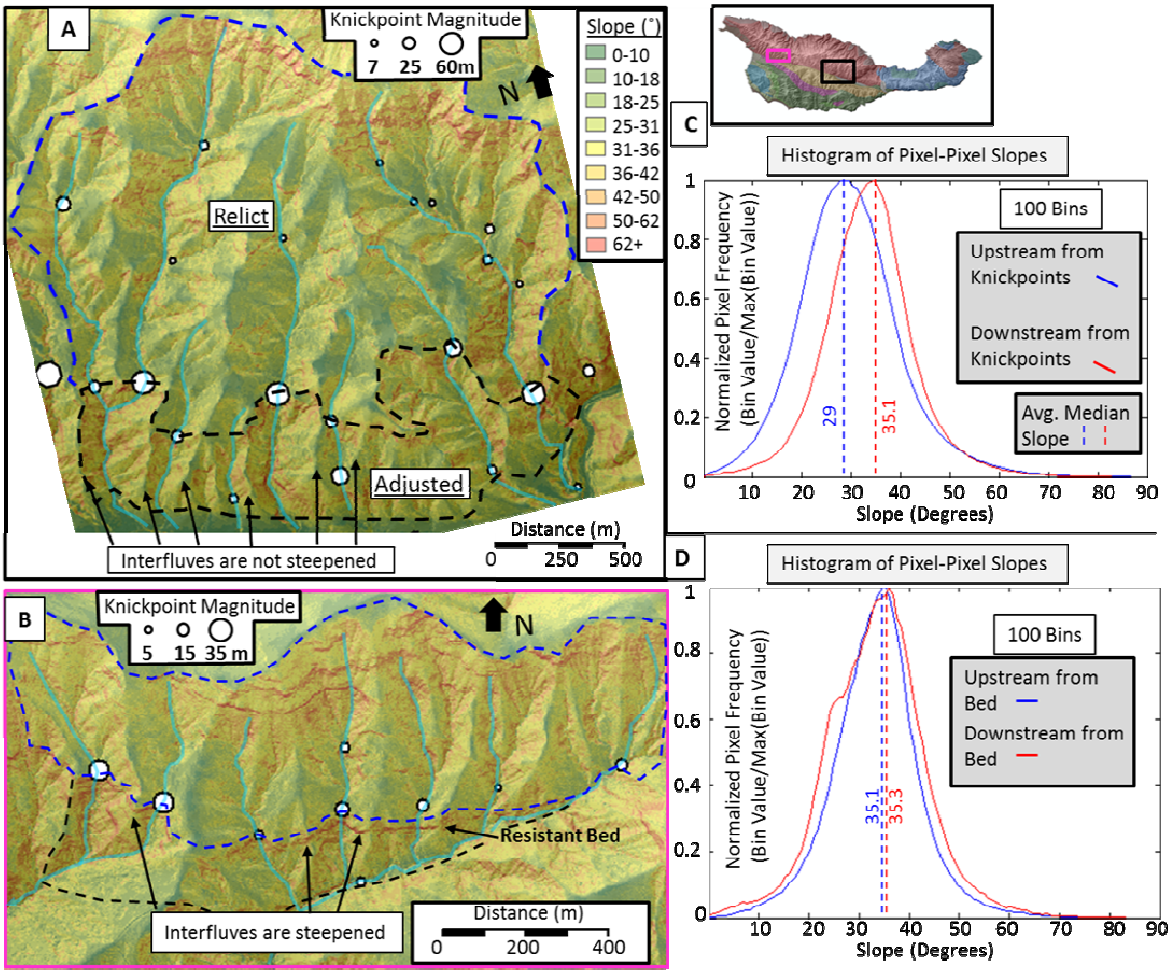

Figure 13) A) Hillslope gradient upstream and downstream from migrating knickpoints (zoomed in from Fig. 12) B) Hillslope gradient upstream and downstream from a resistant bed that supports knickpoints. C) Histogram of hillslope gradient upstream and downstream from migratory knickpoints regions (labeled in A). Hillslopes downstream from migrating knickpoints are approximately 6˚ steeper than hisllopes upstream from migrating knickpoints. D) Histogram of hillslope gradient upstream and downstream from fixed knickpoints (labeled in B). Hillslopes upstream and downstream from fixed knickpoints have similar slope histogram distributions.

B. ***Impact of DEM Resolution***

Small coastal catchments (Fig. 11A) exhibit a similar landscape steepening downstream from migratory knickpoints (Fig. 14). Using a 1-m LiDAR DEM, hillslope gradient is approximately 5˚ steeper downstream from migratory knickpoints, with 19.3% - 8.7% of the landscape steepened beyond threshold hillslope values (Fig. 14D). Landslide scars, hillslope failures, and debris flow channels are common downstream from the knickpoints (Fig. 14C), whereas these markers are mostly absent upstream from the knickpoints.

When performing the same analysis on the same region with a 10-m resolution DEM, the slope histogram distributions upstream and downstream from the knickpoints are nearly identical and the hillslope signature of stream transience goes undetected (Fig. 14E). These histograms are also substantially different from the histograms calculated from the 1-m DEM [e.g. *Dibiase et al.,* 2010]. In the 10-m DEM slope-histogram, the median slope has decreased relative to the 1-m DEM slope-histogram by 5.3˚ upstream from the knickpoints and even more profoundly in the more narrow canyons downstream from the knickpoints (-10.5˚). The range of slopes also decreases to 48˚. Perhaps a 10-m DEM would be sufficient resolution to distinguish difference in landscape character surrounding larger-scale knickpoints in active orogens; however, at the scale of analysis on Santa Cruz Island, this DEM does not capture a difference in hillslope gradient nor the geomorphic markers of hillslope failures.

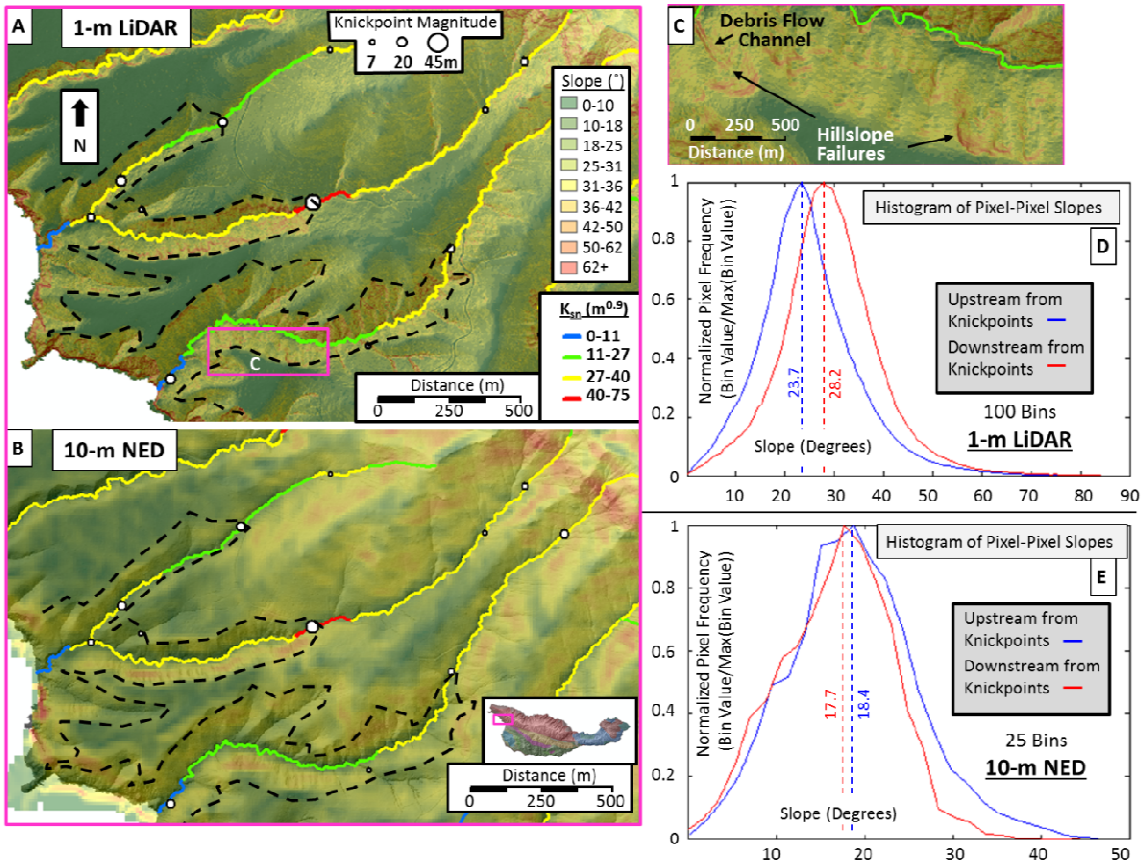

Figure 14) A) A Spatial plot of the streams analyzed in Fig. 11. displaying hillslope gradient calculated from a 1-m DEM. K_{sn} decreases downstream from the knickpoints, which is unexpected and we have little explanation for this pattern. The black dashed line separates the landscape upstream and downstream from the knickpoints. B) Spatial plot of hillslope gradient for the same region calculated from a 10-m DEM. C) A zoomed in view on the pink box from "A" highlights hillslope failures visible in the LiDAR imagery. D) Histogram of hillslope gradient upstream and downstream from migratory knickpoints on the LiDAR 1-m DEM. E) Histogram of hillslope gradient upstream and downstream from migratory knickpoints on the LiDAR 10-m DEM. The number of histogram bins was reduced, because the 10-m DEM has 100 times less pixels in the analysis region and the range of slope values decreased by a factor of 2.

IV. *Conclusion*

New insights arise from both a computer-based algorithm that identifies knickpoints and a high-resolution regional slope map calculated through a 1-m LiDAR DEM. The algorithm rapidly contextualizes a large dataset of knickpoints across a landscape that exhibits spatial variations in bedrock geology, baselevel-fall, and stream-catchment geometry. A regional slope map calculated on a 1-m resolution DEM reveals discontinuities in hillslope gradient

upstream and downstream from migratory knickpoints. These observations can be used to estimate knickpoint mobility, landscape response form, regional susceptibility to geological hazards, and the timing and manor of regional environmental changes. Many observations and hypotheses can be constructed solely from the results of these tools, even in landscapes that lack well-characterized geochronology. Given a well constrained geochronology, time-space substitution can be made to study hillslope response to baselevel fall as a knickpoint migrates upstream at a known rate. More precise volumetric calculations between reconstructed stream profiles and the current-adjusting surface could be used to estimate volumes of eroded material during transient knickpoint migration. With a few dated surfaces, the rates and fluxes at which stream transience operates could be quantified and these processes can be accounted for in mass-balance studies that relate overall erosion rates and offshore deposition.

Similar computer algorithms could be constructed to identify systematic changes in hillslope angle, channel sinuosity, or channel widths to characterize three-dimensional variations in stream networks around knickpoints rather than just two. These insights would improve coupling analyses between hillslopes and stream channels and may further improve both knickpoint identification and characterizing knickpoint behavior. Ideally, this software could be used to rapidly identify knickpoints and test the applicability of stream-power-based knickpoint retreat models. Differences between actual knickpoint locations and predictions from a knickpoint retreat model will highlight potential shortcomings in these predictive tools and moreover, strengthen our understanding of how landscapes adjust to external forcing in a variety of environments and how stream networks relay information upstream through migratory signals.

References

1. Abbühl, L. M., K. P. Norton, J. D. Jansen, F. Schlunegger, A. Aldahan, and G. Possnert (2011), Erosion rates and mechanisms of knickzone retreat inferred from 10Be measured across strong climate gradients on the northern and central Andes Western Escarpment, *Earth Surface Processes and Landforms*, *36*(11), 1464-1473.

2. Baldwin, J. A., Whipple, K. X., & Tucker, G. E. (2003). Implications of the shear stress river incision model for the timescale of postorogenic decay of topography. *Journal of Geophysical Research*: Solid Earth (1978–2012), 108(B3).

3. Berlin, M. M., and R. S. Anderson (2007), Modeling of knickpoint retreat on the Roan Plateau, western Colorado, *Journal of Geophysical Research: Earth Surface (2003–2012)*, *112*(F3).

4. Berlin, M. M., & Anderson, R. S. (2009). Steepened channels upstream of knickpoints: Controls on relict landscape response. *Journal of Geophysical Research: Earth Surface (2003–2012)*, 114(F3).

5. Bigi, A., L. E. Hasbargen, A. Montanari, and C. Paola (2006), Knickpoints and hillslope failures: Interactions in a steady-state experimental landscape, *Geological Society of America Special Papers*, *398*, 295-307.

6. Bishop, P., T. B. Hoey, J. D. Jansen, and I. L. Artza (2005), Knickpoint recession rate and catchment area: the case of uplifted rivers in Eastern Scotland, *Earth Surface Processes and Landforms*, *30*(6), 767-778.

7. Booth, D. B. (1990), Stream channel incision following drainage basin urbanization, *JAWRA Journal of the American Water Resources Association*, *26*(3), 407-417.

8. Brocard, G., and P. Van der Beek (2006), Influence of incision rate, rock strength, and bedload supply on bedrock river gradients and valley-flat widths: Field-based evidence and calibrations from western Alpine rivers (southeast France), *Geological Society of America Special Papers*, *398*, 101-126.

9. Burbank, D. W., & Anderson, R. S. (2011). Tectonic geomorphology. *John Wiley & Sons*.

10. Burbank, D. W., Leland, J., Fielding, E., Anderson, R. S., Brozovic, N., Reid, M. R., & Duncan, C. (1996). Bedrock incision, rock uplift and threshold hillslopes in the northwestern Himalayas. *Nature*, 379(6565), 505-510.

11. Carson, M. A., & Petley, D. J. (1970). The existence of threshold hillslopes in the denudation of the landscape. *Transactions of the Institute of British Geographers*, 71-95.

12. Castillo, M., P. Bishop, and J. D. Jansen (2013), Knickpoint retreat and transient

bedrock channel morphology triggered by base-level fall in small bedrock river catchments: The case of the Isle of Jura, Scotland, *Geomorphology*, *180*, 1-9.

13. Chaytor, J. D., C. Goldfinger, M. A. Meiner, G. J. Huftile, C. G. Romsos, and M. R. Legg (2008), Measuring vertical tectonic motion at the intersection of the Santa Cruz–Catalina Ridge and Northern Channel Islands platform, California Continental Borderland, using submerged paleoshorelines, *Geological Society of America Bulletin*, *120*(7-8), 1053-1071.

14. Clark, M. K., Maheo, G., Saleeby, J., and Farley, K. A., 2005, The non-equilibrium landscape of the southern Sierra Nevada, California: *GSA Today*, v. 15, p. 4-10.

15. Cook, K. L., J. M. Turowski, and N. Hovius (2013), A demonstration of the importance of bedload transport for fluvial bedrock erosion and knickpoint propagation, *Earth Surface Processes and Landforms*, *38*(7), 683-695.

16. Crosby, B. T., and K. X. Whipple (2006), Knickpoint initiation and distribution within fluvial networks: 236 waterfalls in the Waipaoa River, North Island, New Zealand, *Geomorphology*, *82*(1), 16-38.

17. DiBiase, R. A., K. X. Whipple, A. M. Heimsath, and W. B. Ouimet (2010), Landscape form and millennial erosion rates in the San Gabriel Mountains, CA, *Earth and Planetary Science Letters*, *289*(1), 134-144.

18. DiBiase, R. A., and K. X. Whipple (2011), The influence of erosion thresholds and runoff variability on the relationships among topography, climate, and erosion rate, *Journal of Geophysical Research: Earth Surface (2003–2012)*, *116*(F4).

19. DiBiase, R. A., Heimsath, A. M., & Whipple, K. X. (2012). Hillslope response to tectonic forcing in threshold landscapes. *Earth Surface Processes and Landforms*, 37(8), 855-865.

20. DiBiase, R. A., K. X. Whipple, M. P. Lamb, and A. M. Heimsath (2014), The role of waterfalls and knickzones in controlling the style and pace of landscape adjustment in the western San Gabriel Mountains, California, *Geological Society of America Bulletin*, B31113. 31111.

21. Dibblee, T. W. (1991). Geologic Map of Eastern Santa Cruz Island, Santa Barbara County, California. J. A. Minch (Ed.). *Dibblee Geological Foundation.*

22. Duvall, A., E. Kirby, and D. Burbank (2004), Tectonic and lithologic controls on bedrock channel profiles and processes in coastal California, *Journal of Geophysical Research: Earth Surface (2003–2012)*, *109*(F3).

23. Flint, J. (1974), Stream gradient as a function of order, magnitude, and discharge, *Water Resources Research*, *10*(5), 969-973.

24. Foster, Melissa A., and Harvey M. Kelsey. "Knickpoint and knickzone formation and propagation, South Fork Eel River, northern California." *Geosphere* 8.2 (2012): 403-416.

25. Frankel, K. L., F. J. Pazzaglia, and J. D. Vaughn (2007), Knickpoint evolution in a vertically bedded substrate, upstream-dipping terraces, and Atlantic slope bedrock channels, *Geological Society of America Bulletin*, *119*(3-4), 476-486.

26. Gardner, T. W. (1983), Experimental study of knickpoint and longitudinal profile evolution in cohesive, homogeneous material, *Geological Society of America Bulletin*, *94*(5), 664-672.

27. Gallen, S. F., K. W. Wegmann, K. L. Frankel, S. Hughes, R. Q. Lewis, N. Lyons, P. Paris, K. Ross, J. B. Bauer, and A. C. Witt (2011), Hillslope response to knickpoint migration in the Souther Appalachians: implications for the evolution of post-orogenic landscapes, *Earth Surface Processes and Landforms,* 36(9), 1254-1267.

28. Gonga-Saholiariliva, N., Y. Gunnell, D. Harbor, and C. Mering (2011), An automated method for producing synoptic regional maps of river gradient variation: Procedure, accuracy tests, and comparison with other knickpoint mapping methods, *Geomorphology*, *134*(3–4), 394-407.

29. Gurrola, L. D., Keller, E. A., Chen, J. H., Owen, L. A., & Spencer, J. Q. (2014). Tectonic geomorphology of marine terraces: Santa Barbara fold belt, California. *Geological Society of America Bulletin*, 126(1-2), 219-233.

30. Hack, J. T. (1957), Studies of longitudinal stream profiles in Virginia and Maryland.

31. Hanks, T. C., and R. H. Webb (2006), Effects of tributary debris on the longitudinal profile of the Colorado River in Grand Canyon, *Journal of Geophysical Research: Earth Surface (2003–2012)*, *111*(F2).

32. Harkins, N., E. Kirby, A. Heimsath, R. Robinson, and U. Reiser (2007), Transient fluvial incision in the headwaters of the Yellow River, northeastern Tibet, China, *Journal of Geophysical Research: Earth Surface (2003–2012)*, *112*(F3).

33. Hasbargen, L. E., & Paola, C. (2000). Landscape instability in an experimental drainage basin. *Geology*, 28(12), 1067-1070.

34. Haviv, I., Y. Enzel, K. Whipple, E. Zilberman, A. Matmon, J. Stone, and K. Fifield (2010), Evolution of vertical knickpoints (waterfalls) with resistant caprock: Insights from numerical modeling, *Journal of Geophysical Research: Earth Surface (2003–2012)*, *115*(F3).

35. Hilley, G. E., and J. R. Arrowsmith (2008), Geomorphic response to uplift along the Dragon's Back pressure ridge, Carrizo Plain, California, *Geology*, *36*(5), 367-370.

36. Howard, A. D., & Kerby, G. (1983). Channel changes in badlands. *Geological Society of America Bulletin*, 94(6), 739-752.

37. Howard, A. D., W. E. Dietrich, and M. A. Seidl (1994), Modeling fluvial erosion on regional to continental scales, *Journal of Geophysical Research: Solid Earth (1978–2012)*, *99*(B7), 13971-13986.

38. Jansen, J. D., D. Fabel, P. Bishop, S. Xu, C. Schnabel, and A. T. Codilean (2011), Does decreasing paraglacial sediment supply slow knickpoint retreat?, *Geology*, *39*(6), 543-546.

39. Kirby, E., & Whipple, K. (2001). Quantifying differential rock-uplift rates via stream profile analysis. *Geology*, 29(5), 415-418.

40. Kirby, E., and K. X. Whipple (2012), Expression of active tectonics in erosional landscapes, *Journal of Structural Geology*, *44*, 54-75.

41. Korup, O. (2006), Rock-slope failure and the river long profile, *Geology*, *34*(1), 45-48.

42. Lague, D. (2014), The stream power river incision model: evidence, theory and beyond, *Earth Surface Processes and Landforms*, *39*(1), 38-61.

43. Lamb, M. P., and W. E. Dietrich (2009), The persistence of waterfalls in fractured rock, *Geological Society of America Bulletin*, *121*(7-8), 1123-1134.

44. Lamb, M. P., N. J. Finnegan, J. S. Scheingross, and L. S. Sklar (2015), New insights into the mechanics of fluvial bedrock erosion through flume experiments and theory, *Geomorphology*.

45. Lambeck, K., Yokoyama, Y., & Purcell, T. (2002). Into and out of the Last Glacial Maximum: sea-level change during Oxygen Isotope Stages 3 and 2. *Quaternary Science Reviews*, 21(1), 343-360.

46. Loget, N., and J. Van Den Driessche (2009), Wave train model for knickpoint migration, *Geomorphology*, *106*(3), 376-382.

47. Mackey, B. H., J. S. Scheingross, M. P. Lamb, and K. A. Farley (2014), Knickpoint formation, rapid propagation, and landscape response following coastal cliff retreat at the last interglacial sea-level highstand: Kaua ‘i, Hawai ‘i, *Geological Society of America Bulletin*, *126*(7-8), 925-942.

48. Marshall, J. A., and J. J. Roering (2014), Diagenetic variation in the Oregon Coast Range: Implications for rock strength, soil production, hillslope form, and landscape evolution, *Journal of Geophysical Research: Earth Surface*, *119*(6), 1395-1417.

49. Miller, J. R. (1991), The influence of bedrock geology on knickpoint development

and channel-bed degradation along downcutting streams in south-central Indiana, *The Journal of Geology*, 591-605.

50. Miller, S. R., S. L. Baldwin, and P. G. Fitzgerald (2012), Transient fluvial incision and active surface uplift in the Woodlark Rift of eastern Papua New Guinea, *Lithosphere*, *4*(2), 131-149.

51. Miller, S. R., P. B. Sak, E. Kirby, and P. R. Bierman (2013), Neogene rejuvenation of central Appalachian topography: Evidence for differential rock uplift from stream profiles and erosion rates, *Earth and Planetary Science Letters*, *369*, 1-12.

52. Montgomery, D. R., and E. Foufoula-Georgiou (1993), Channel network source representation using digital elevation models, *Water Resources Research, 29*(12), 3925-3934.

53. Montgomery, D. R., & Brandon, M. T. (2002). Topographic controls on erosion rates in tectonically active mountain ranges. *Earth and Planetary Science Letters*, 201(3), 481-489.

54. Moore, L. J., Benumof, B. T., & Griggs, G. B. (1999). Coastal erosion hazards in Santa Cruz and San Diego Counties, California. *Journal of Coastal Research*, 121-139.

55. Muhs, D. R., Simmons, K. R., Schumann, R. R., Groves, L. T., Mitrovica, J. X., & Laurel, D. (2012). Sea-level history during the Last Interglacial complex on San Nicolas Island, California: implications for glacial isostatic adjustment processes, paleozoogeography and tectonics. *Quaternary Science Reviews*, 37, 1-25.

56. Muhs, D. R., Simmons, K. R., Schumann, R. R., Groves, L. T., DeVogel, S. B., Minor, S. A., & Laurel, D. (2014). Coastal tectonics on the eastern margin of the Pacific Rim: late Quaternary sea-level history and uplift rates, Channel Islands National Park, California, USA. *Quaternary Science Reviews*, 105, 209-238.

57. Nardin, T. R., Osborne, R. H., Bottjer, D. J., & Scheidemann, R. C. (1981). Holocene sea-level curves for Santa Monica shelf, California continental borderland. *Science*, 213(4505), 331-333.

58. Niemann, J. D.*,* N. M. Gasparini*,* G. E. Tucker*, and* R. L. Bras *(*2001*),* A quantitative evaluation of Playfair's law and its use in testing long-term stream erosion models*, Earth Surf. Processes Landforms,* 26*,* 1317–1332.

59. Nolf, B., and P. Nolf (1969), Santa Cruz Island Volcanics.

60. Ouimet, W. B., K. X. Whipple, L. H. Royden, Z. Sun, and Z. Chen (2007), The influence of large landslides on river incision in a transient landscape: Eastern margin of the Tibetan Plateau (Sichuan, China), *Geological Society of America Bulletin*, *119*(11-12), 1462-1476.

61. Patterson, R. H. (1979). Tectonic Geomorphology and Neotectonics of the Santa Cruz Island Fault Santa Barbara County, California *(Doctoral dissertation, University of California, Santa Barbara)*.

62. Prancevic, J. P., and Lamb, M. P., 2015, Unraveling bed slope from relative roughness in initial sediment motion: *Journal of Geophysical Research*: Earth Surface, v. 120, no. 3, p. 474-489.

63. Perroy, R. L., B. Bookhagen, G. P. Asner, and O. A. Chadwick (2010), Comparison of gully erosion estimates using airborne and ground-based LiDAR on Santa Cruz Island, California, *Geomorphology*, *118*(3), 288-300.

64. Perron, J. T., and L. Royden (2013), An integral approach to bedrock river profile analysis, *Earth Surface Processes and Landforms*, *38*(6), 570-576.

65. Pinter, N., S. B. Lueddecke, E. A. Keller, and K. R. Simmons (1998a), Late quaternary slip on the Santa Cruz Island fault, California, *Geological Society of America Bulletin*, *110*(6), 711-722.

66. Pinter, N., C. C. Sorlien, and A. T. Scott (1998b), Late Quaternary folding and faulting of Santa Cruz Island, California.

67. Pinter, N., Johns, B., Little, B., & Vestal, W. D. (2001). Fault-related folding in California's Northern Channel Islands documented by rapid-static GPS positioning. *GSA TODAY*, 11(5), 4-9.

68. Pinter, N., C. C. Sorlien, and A. T. Scott (2003), Fault-related fold growth and isostatic subsidence, California Channel Islands, *American Journal of Science*, *303*(4), 300-318.

69. Prince, P. S., J. A. Spotila, and W. S. Henika (2011), Stream capture as driver of transient landscape evolution in a tectonically quiescent setting, *Geology*, *39*(9), 823-826.

70. Queiroz, G. L., E. Salamuni, and E. R. Nascimento (2015), Knickpoint finder: A software tool that improves neotectonic analysis, *Computers & Geosciences*, *76*(0), 80-87.

71. Rockwell, T. K. (1992). Ages and Deformation of Marine Terraces Between Point Conception and Gaviota: Western Transverse Ranges, California.

72. Savitzky, A., & Golay, M. J. (1964). Smoothing and differentiation of data by simplified least squares procedures. *Analytical chemistry*, 36(8), 1627-1639.

73. Schmidt, K. M., & Montgomery, D. R. (1995). Limits to relief. *Science*, 270(5236), 617.

74. Schwanghart, W., and D. Scherler (2014), Short Communication: TopoToolbox 2–MATLAB-based software for topographic analysis and modeling in Earth surface sciences, *Earth Surface Dynamics*, *2*(1), 1-7.

75. Seeber, L., and C. C. Sorlien (2000), Listric thrusts in the western Transverse Ranges, California, *Geological Society of America Bulletin*, *112*(7), 1067-1079.

76. Seidl, M. A., R. C. Finkel, M. W. Caffee, G. B. Hudson, and W. E. Dietrich (1997), Cosmetic Isotope Analyses Applied to River Longitudinal Profile Evolution: Problems and Interpretations, *Earth Surface Processes and Landforms*, *22*(3), 195-209.

77. Shaw, J. H., and J. Suppe (1994), Active faulting and growth folding in the eastern Santa Barbara Channel, California, *Geological Society of America Bulletin*, *106*(5), 607-626.

78. Sklar, L. S., and W. E. Dietrich (2001), Sediment and rock strength controls on river incision into bedrock, *Geology*, *29*(12), 1087-1090.

79. Snyder, N. P., K. X. Whipple, G. E. Tucker, and D. J. Merritts (2000), Landscape response to tectonic forcing: Digital elevation model analysis of stream profiles in the Mendocino triple junction region, northern California, *Geological Society of America Bulletin*, *112*(8), 1250-1263

80. Synder, N. P., K. X. Whipple, G. Tucker, and D. Merritts (2002), Interactions between onshore bedrock-channel incision and nearshore wave-base erosion forced by eustasy and techtonics, *Basin Research, 14*(2), 105-127.

81. Sorlien, C. C. (1994). Faulting and uplift of the northern Channel Islands, California. In The fourth California Islands symposium: update on the status of resources (pp. 282-296). *Santa Barbara Museum of Natural History.*

82. Stein, R. S., King, G. C. P., and Rundel, J. B., 1988, The growth of geological structure by repeated earthquakes 2. Field examples of continental dip-slip faults: *Journal of Geophysical Research*, v. 93, p. 13,319-313,331.

83. Tinkler, K. J., J. W. Pengelly, G. Asselin, and W. G. Parkins (1994), Postglacial recession of Niagara Falls in relation to the Great Lakes, *Quaternary Research*, *42*(1), 20-29.

84. Trecker, M. A., Gurrola, L. D., & Keller, E. A. (1999). Oxygen-isotope correlation of marine terraces and uplift of the Mesa Hills, Santa Barbara, California, USA. *Geological Society, London, Special Publications,* 146(1), 57-69.

85. Tsou, C. Y., Chigira, M., Matsushi, Y., & Chen, S. C. (2014). Fluvial incision history that controlled the distribution of landslides in the Central Range of Taiwan. *Geomorphology*, 226, 175-192.

86. Wang, Z., Cui, P., Yu, G. A., & Zhang, K. (2012). Stability of landslide dams and development of knickpoints. *Environmental Earth Sciences*, 65(4), 1067-1080.

87. Weaver, D. W., and G. L. Meyer (1969), Stratigraphy of northeastern Santa Cruz Island. *AAPG Pacific Section.,* 2009, 94–105.

88. Weaver, D., & Nolf, B. (1969). Geology of Santa Cruz Island (map). Geology of the northern Channel Islands, southern California borderland: *PacificSection, American Association of Petroleum Geologists Special Publication*, scale, 1(24), 000.

89. Whipple, K. X., and G. E. Tucker (1999), Dynamics of the stream-power river incision model: Implications for height limits of mountain ranges, landscape response timescales, and research needs, *Journal of Geophysical Research: Solid Earth (1978-2012), 104*(B8), 17661-17674.

90. Whipple, K. X. (2004), Bedrock rivers and the geomorphology of active orogens, *Annu. Rev. Earth Planet. Sci.*, *32*, 151-185.

91. Whittaker, A. C., P. A. Cowie, M. Attal, G. E. Tucker, and G. P. Roberts (2007), Bedrock channel adjustment to tectonic forcing: Implications for predicting river incision rates, *Geology*, *35*(2), 103-106.

92. Whittaker, A. C., and S. J. Boulton (2012), Tectonic and climatic controls on knickpoint retreat rates and landscape response times, *Journal of Geophysical Research: Earth Surface (2003–2012)*, *117*(F2).

93. Whittaker, A. C., and A. S. Walker (2014), Geomorphic constraints on fault throw rates and linkage times: Examples from the Northern Gulf of Evia, Greece, *Journal of Geophysical Research: Earth Surface.*

94. Wobus, C., K. X. Whipple, E. Kirby, N. Snyder, J. Johnson, K. Spyropolou, B. Crosby, and D. Sheehan (2006a), Tectonics from topography: Procedures, promise, and pitfalls, *Geological Society of America Special Papers*, *398*, 55-74.

95. Wobus, C. W., B. T. Crosby, and K. X. Whipple (2006b), Hanging valleys in fluvial systems: Controls on occurrence and implications for landscape evolution, *Journal of Geophysical Research: Earth Surface (2003–2012)*, *111*(F2).

96. Yanites, B. J., G. E. Tucker, K. J. Mueller, and Y.-G. Chen (2010a), How rivers react to large earthquakes: Evidence from central Taiwan, *Geology*, *38*(7), 639-642.

97. Zaprowski, B. J., E. B. Evenson, F. J. Pazzaglia, and J. B. Epstein (2001), Knickzone propagation in the Black Hills and northern High Plains: A different perspective on

the late Cenozoic exhumation of the Laramide Rocky Mountains, *Geology*, *29*(6), 547-550.

Appendix

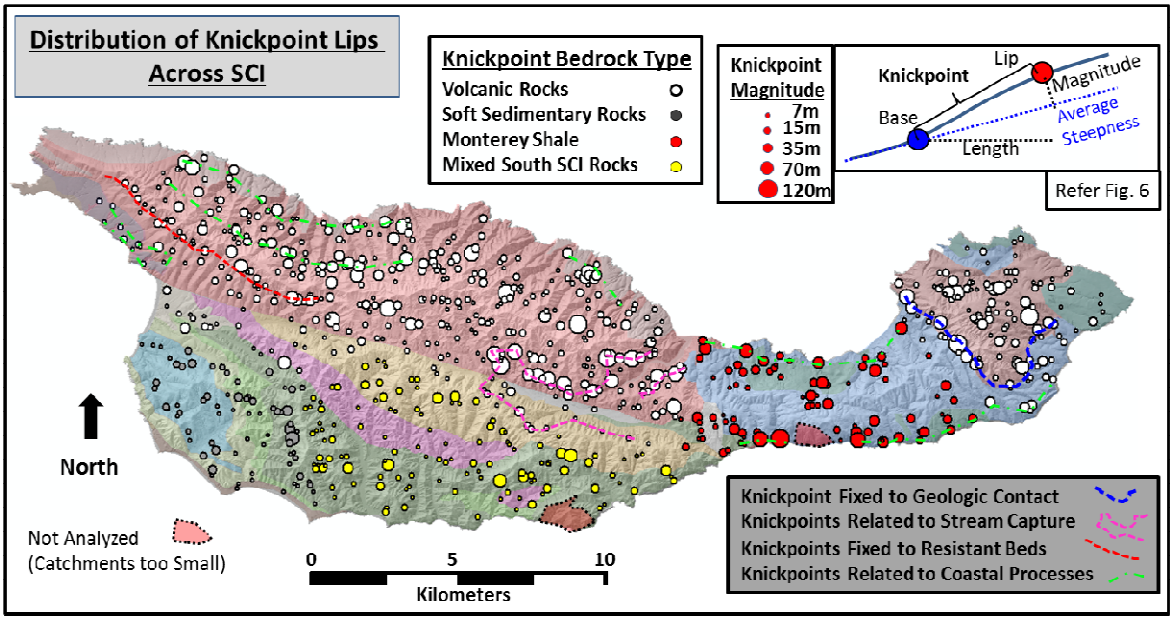

Supplementary Figure 1) Spatial plot of knickpoint lips located by algorithm, knickpoints are color coordinated by general bedrock lithology type. Marker size reflects knickpoint magnitude. We label certain knickpoints that are generated from various mechanisms highlighted in this paper.

A. *Additional Figures Demonstrating Hillslope behavior around Knickpoints*

Slope histograms were calculated on regions upstream and downstream from knickpoints related to a geological contact between Monterey Shale and SCI Volcanics (Supplementary Fig. 1; Fig. 8). The median slope is similar in both regions, suggesting rather fixed knickpoints. The maximum slopes are also similar; however, the downstream polygon contains a significant portion of terraced area exhibiting low slopes

(<10˚).

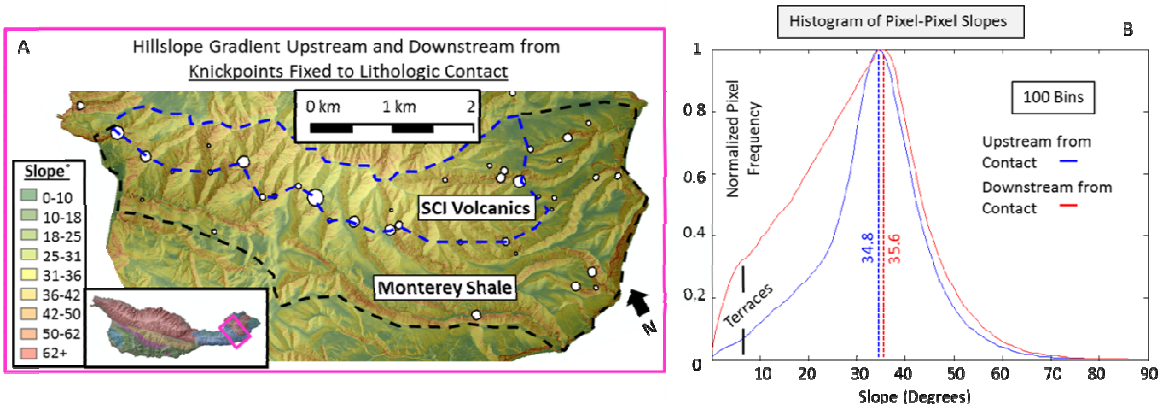

Supplementary Figure 2) Slope histograms for regions upstream (blue) from knickpoints fixed to a geologic contact, and downstream (red) from knickpoints fixed to a geologic contact.

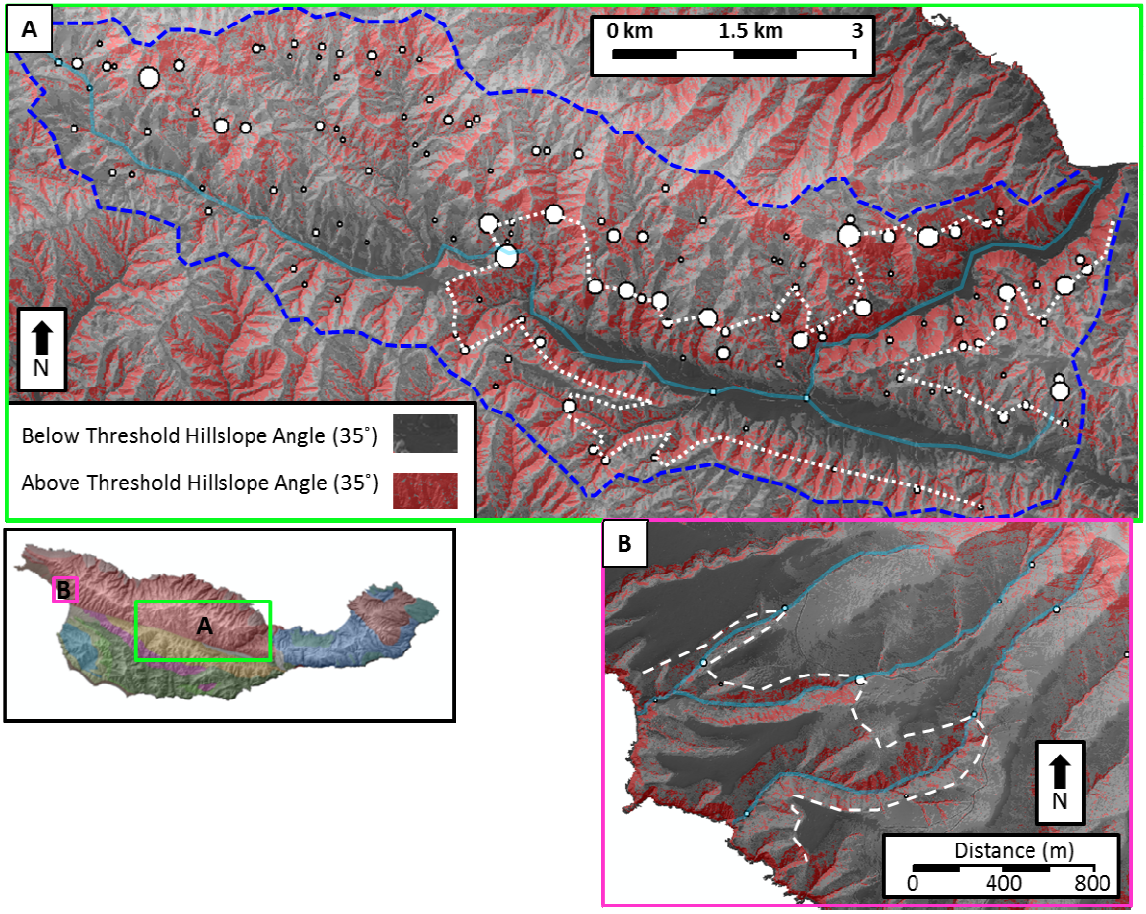

Supplementary Figure 3) Spatial map displaying relationship between knickpoint position and abundance of hillslopes above threshold angles (35˚): A) Landscape upstream and downstream from knickpoints related to central valley stream capture event, B) Landscape upstream and downstream from coastal knickpoints related to baselevel fall and sea-cliff retreat.

B. ***Smoothing during Automated Knickpoint Selection***

A series of filters are used to analyze the de-trended chi plot to correctly select significant inflection points that delineate knickpoint bounds (Fig. 6C). First, some noise resulting from channel roughness, small bedrock steps, or DEM artifacts must be smoothed from the original longitudinal profile in order that larger knickpoint features spanning 10s-100s of cells on a DEM can be measured. A Savitzky-Golay [1964] filter works better than a standard moving-average filter to remove scatter from topographic noise, yet retain "edges" at sharp knickpoint inflection points (compare blue and black curves, Supplementary Fig. 2). After an initial smoothing, measurements of knickpoint dimensions permit calculation of an appropriate minimum knickpoint magnitude or slope. Convexities in a longitudinal profile with a magnitude or slope smaller than a specified condition can be filtered out of an analysis.

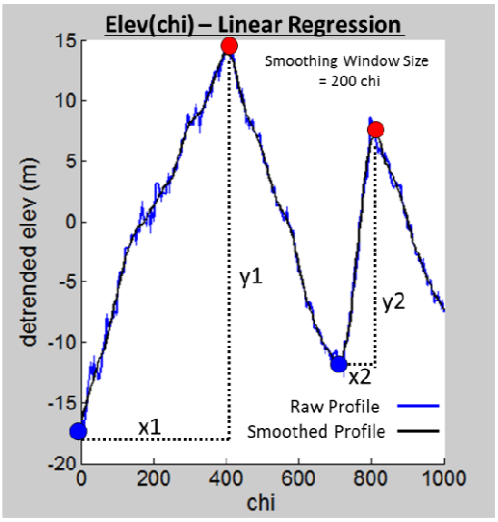

Supplementary Figure 4) Example of a de-trended chi plot before (blue) and after (black) smoothing the profile with a Savitzky-Golay filter, the filter length scale was 200 cells in this example. Cells vary in size with different DEM resolution, and the smoothing window length scale typically requires some degree of calibration with manually selected knickpoints [using *Wobus et al.,* 2006a].

In some reaches, multiple small knickpoints are closely spaced and, taken together, would outline a larger scale knickpoint (Supplementary Fig. 5B-D). To address such situations, an additional 'lumping' function scans potential identified knickpoints that are larger than the minimum knickpoint size, and if the knickpoints found are within a certain distance from one another, the knickpoints are combined. The magnitudes for such amalgamated knickpoints are summed, and the bounds of the knickpoint are extended to the lip of the upstream knickpoint and the base of the downstream knickpoint (Supplementary Fig. 5).

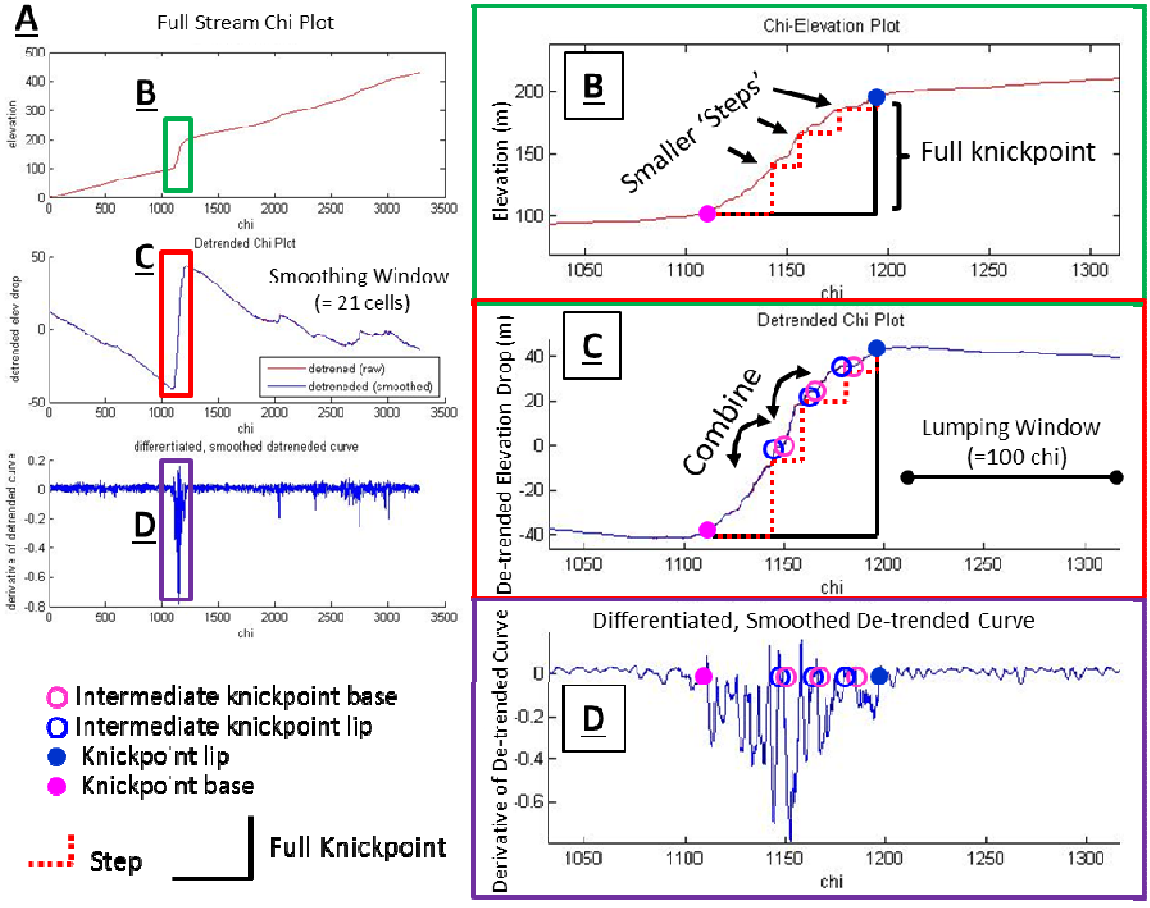

Supplementary Figure 5) Demonstration of the knickpoint lumping function: A chi plot, de-trended chi plot, and differentiated de-trended chi plot are shown for a full stream (A) and a large knickpoint (B-D) that encompasses smaller knickpoint steps (B-C). These small steps are each bounded by negative-to-positive and positive-to-negative inflection points in the differentiated de-trended chi plot (D) and contain significant de-

trended elevation drops (C). Because these steps are spaced closer than the lumping window distance of 100 chi, the steps are combined into one full, larger knickpoint (B).

After combining closely spaced smaller knickpoints, a second minimum knickpoint magnitude threshold can be applied to remove knickpoints that did not grow past a certain magnitude. Similarly, an optional filter can be applied to eliminate knickpoints which do not exceed a certain steepness threshold. The steepness threshold allows users to identify only very steep knickpoints, such as waterfalls, if desired.

The system introduces flexibility through relatively few conditions. Studies focusing on fine-scale erosional processes around waterfalls can set conditions biased towards the geometries of waterfalls: a low minimum knickpoint size, a small knickpoint lumping distance, and a high steepness threshold; whereas studies focusing on regional signal propagation and landscape adjustment can set larger minimum knickpoint size and a longer knickpoint lumping distance to analyze broader features.

C. *Calibration during Automated Knickpoint Selection*

To select the appropriate smoothing parameters for a particular study scale, knickpoints can be manually selected on a trunk-stream longitudinal profile using techniques described in *Wobus et al.,* [2006a]. A calibration script then compares the position of the manually-selected knickpoints to the position of algorithm-selected knickpoints in the same catchment for a suite of parameter combinations (Supplementary Fig. 6). Ideally, all of the knickpoints selected individually will lie within a certain allowable error radius from the algorithm selected knickpoints. The allowable error radius should scale with the DEM resolution and

the length of the knickpoints in the study.

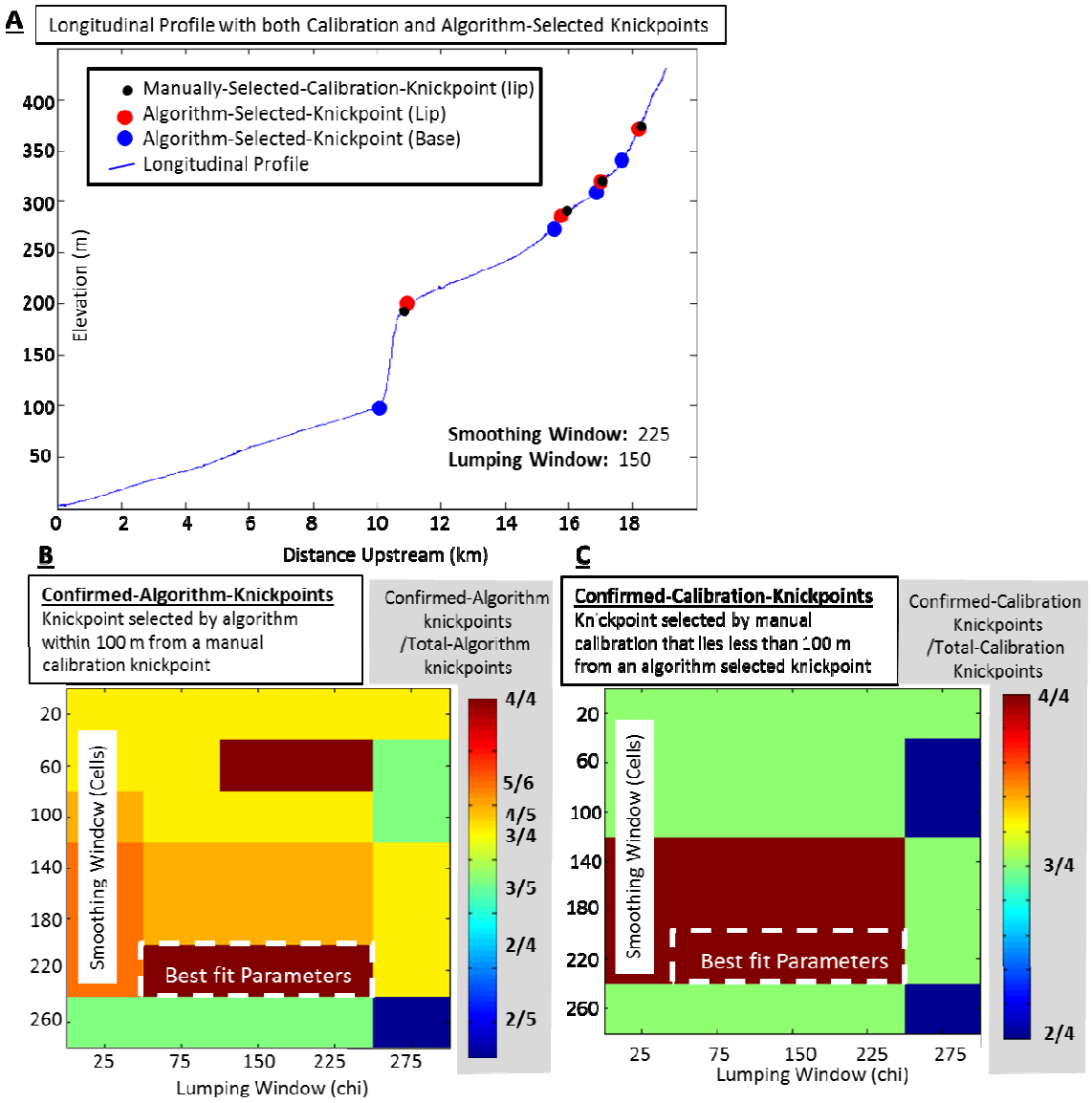

Supplementary Figure 6) A) Example calibration procedures for longitudinal profile smoothing parameters: A) Longitudinal profile of trunk stream showing knickpoints lips selected manually (calibration knickpoints) and knickpoints selected by the algorithm for best-fit parameters. Combinations of "lumping window" and "smoothing window" sizes illustrate the best-fit parameters for matching algorithm-selected (B) versus manually-selected (C) knickpoints. Ideal best-fit parameters should confirm all calibration-knickpoints, all algorithm-knickpoints, and should produce the same number of algorithm-knickpoints as calibration-knickpoints. Note with fractions that have a denominator ≠4 (see "B" above) the algorithm with those smoothing parameter combinations has selected more or less knickpoints than the number of calibration knickpoints (4 in this example).

D. *Field Verification of Knickpoints*

Knickpoints were mapped with a handheld GPS (±5-m accuracy) at the location of the knickpoint scarp visible in the field. Because some knickpoints do not exhibit distinct scarps at the upper bounds of the convex reach [e.g, *Berlin and Anderson,* 2009], the position of the knickpoint scarp may not be the most accurate location of the upper bound of the knickpoint; however, we do expect the knickpoint scarp to lie somewhere between the upstream and downstream bounds of the knickpoint identified by the algorithm.

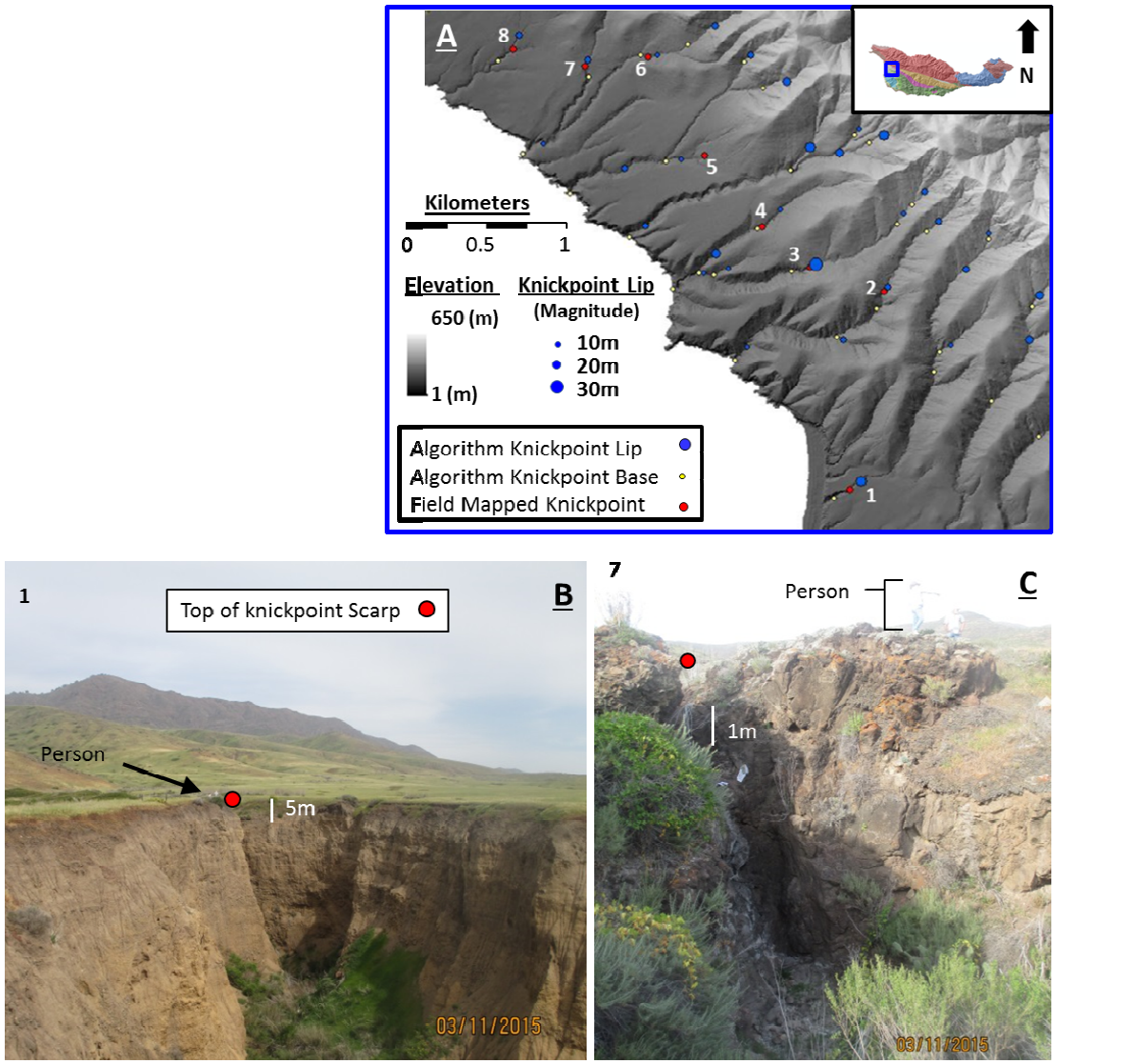

Supplementary Figure 7) Field verification of algorithm knickpoints: A) Location of field verified knickpoints (red dots, numbered 1-8). All field knickpoint scarps were found between the bounds of a knickpoint lip and downstream knickpoint base with the exception of knickpoint #5. Knickpoint 5 has a small magnitude (~3.2 m) and was likely misidentified in the field below the minimum drainage area threshold of 50,000 m^2. B-C) Field photographs of knickpoints 1 and 7.

E. ***Comparison of Knickpoint Positions Selected from 1-m and 10-m DEMs***

The knickpoint-selection-algorithm plots large magnitude knickpoints (>20 m) in similar positions on both the 1-m-resolution DEM and 10-m-resolution DEM (Supplementary Fig. 8). Selected knickpoint position of smaller knickpoints (<20 m) varies more between DEM resolutions, but these variations are expected because small knickpoints (some ~3 m) are impinging on the data resolution of the 10-m DEM. Here, automated measurements of knickpoint size assist interpretations of knickpoint significance, where small knickpoints may reflect DEM artifacts, small resistant bedrock steps and perhaps should be interpreted with less significance than large knickpoints that typically reflect significant landscape discontinuities. However, it is important to note that the coarsening of DEM resolution can change the position and geometry of flow-accumulation arrays [*e.g. Foster and Kelsey,* 2012], alter locations of drainage divides, and slightly affect the organization of drainage networks (Supplementary Fig. 8 divide-breach-artifact). These artifacts in lower resolution DEMs may generate false, large knickpoints, but the mapped position of these knickpoints should reveal whether or not these features result from artifacts in flow-accumulation generation.

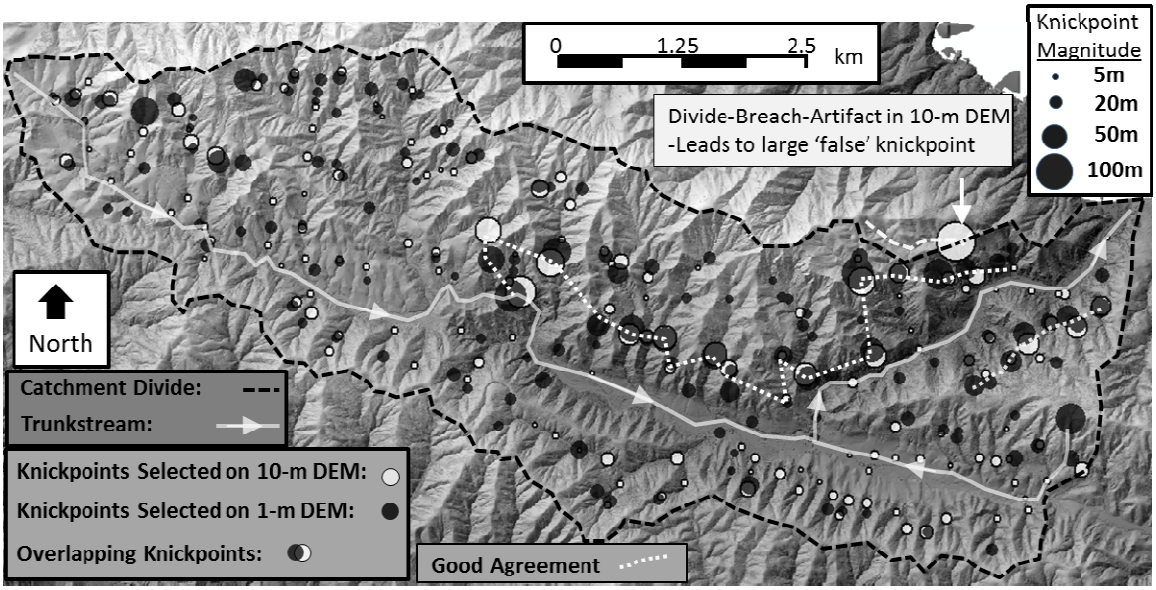

Supplementary Figure 8) Comparison of knickpoint positions selected using DEMs with different resolutions. A grayish-white dotted line highlights large, significant knickpoints that are generally plotted in the same location regardless of DEM resolution; however, DEM resolution can significantly change the position of smaller knickpoints. Also, note the divide-breach-artifact (large white knickpoint) near the northeast side of the catchment. The stream network constructed from the 10-m DEM incorporates a portion of an external stream (thick-dashed, grey-white line) into the catchment bounds of the 1-m resolution DEM (black dashed line).

F. *Quantifying the Accuracy of the Knickpoint Dimensions Measured by Algorithm*

To test the reliability of knickpoint measurements (magnitude, length, and slope), we construct 'synthetic' longitudinal chi plots containing knickpoints with a prescribed geometry (Supplementary Fig. 9). This longitudinal profile is perturbed with a noise function to simulate channel roughness and artifacts within a DEM. The knickpoint selection function is applied to the synthetic chi plot, and the output measurements from the knickpoint selection function were compared to the prescribed knickpoint size (Supplementary Fig. 9). Because the random noise function generates a slightly different profile for each iteration, we run the measurement comparison for 500 iterations to return an average measurement accuracy for each prescribed knickpoint. Additionally, we loop through different smoothing window sizes to characterize the loss of accuracy at larger smoothing window sizes. We find that measurements of knickpoint magnitude are generally

very reliable (measurements are ±5% of actual values for even the largest smoothing windows, Supplementary Fig. 9D); however, measurements of knickpoint slope and length decrease in accuracy substantially when using larger smoothing windows (measurements are ±25% of actual values for the largest smoothing windows, Supplementary Fig. 9E-F).

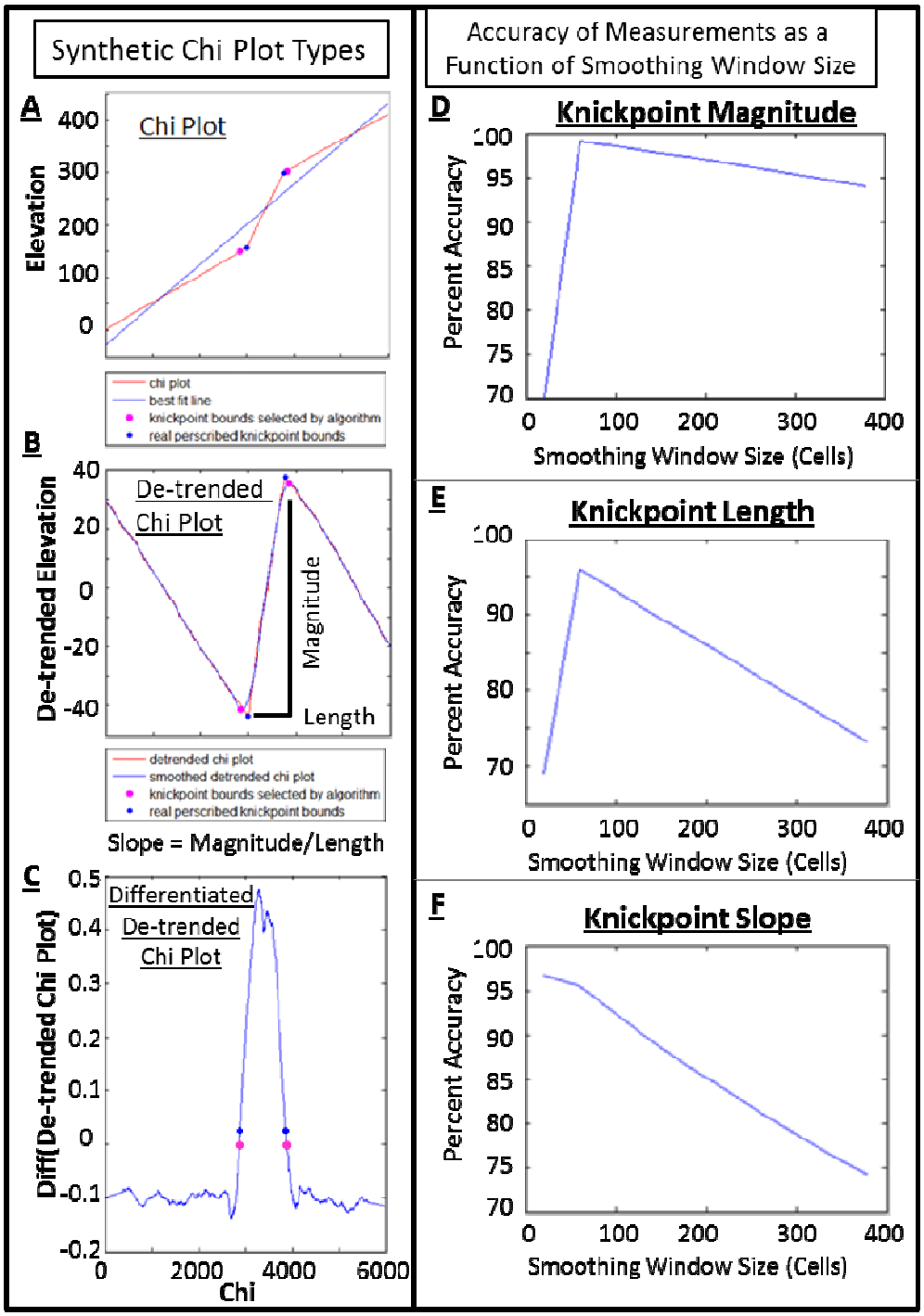

Supplementary Figure 9) Tests in knickpoint measurement accuracy over varying smoothing window sizes: A-C) knickpoint selection process on the same synthetic chi plot with a prescribed knickpoint. D-F) Resulting knickpoint measurement accuracies as a function of smoothing window size.

G. ***A Potential Lithologic Control on Knickpoint Slope*** Additional analyses performed on SCI studied bulk trends in knickpoint slope. Interestingly, knickpoint slopes seem to vary

considerably depending on the lithology supporting the knickpoint. On average, the steepest knickpoints are observed in the harder lithologies (volcanic rocks) and knickpoint slopes are more gradual in softer rocks (Supplementary Fig. 10A). This supports findings by *Frankel et al.,* [2007] and *Gardner,* [1983]; however, the smoothing of the longitudinal profiles during knickpoint selection tends to reduce knickpoint slope by diffusing abrupt knickpoint lips and bases (Supplementary Fig. 9F). This affect is more significant in smaller knickpoints than larger knickpoints, so knickpoint magnitude also tends to affect measurements of knickpoint slope. Dually, knickpoints in the volcanic bedrock tend to have the largest magnitude as well, so in this study, it is challenging to identify to what extent the knickpoint slope measurements are biased by changes in knickpoint magnitude and to what extent the knickpoint slopes actually differ between the harder and softer lithologies.

Additionally, knickpoints developed in the Monterey Shale seem to diffuse (or reduce their slopes) upstream (Supplementary Fig. 10B), assuming that knickpoints further upstream in the Monterey Shale have migrated further and did not develop in-situ. This would be a substantial observation, but again could be biased by the dependency of knickpoint slope on knickpoint magnitude and potentially the frequency of knickpoints at a particular distance upstream (Supplementary Fig. 10D).

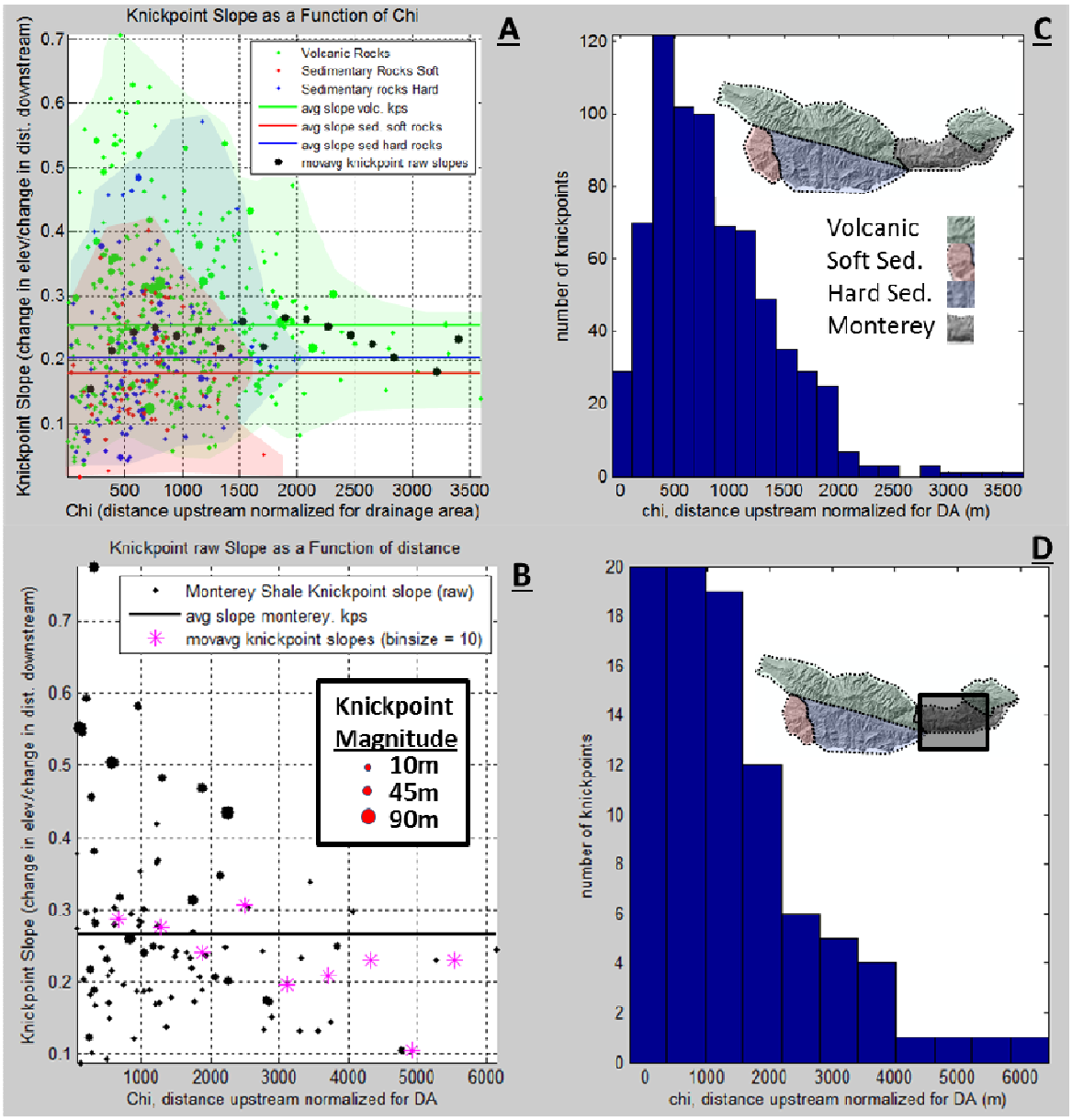

Supplementary Figure 10) A) Bulk distributions of knickpoint slope grouped by lithology. Average knickpoint slope (black dots) remains relatively constant as a function of distance upstream (increasing chi). B) Knickpoint slope decreases as a function of distance upstream for knickpoints in the Monterey Shale, but knickpoint magnitude and frequency (D) also decrease as distance upstream increases.